Biogeosciences
Discussions

1

Modelling Nitrification Inhibitor Effects on N_2O Emissions after Fall and Spring-Applied Slurry by Reducing Nitrifier NH_4^+ Oxidation Rate

Grant, Robert.F.[1*], Lin, Sisi[1] and Hernandez-Ramirez, Guillermo[1]

[1] *Department of Renewable Resources, University of Alberta, Edmonton, AB,*

Canada T6G 2E3

ABSTRACT

Reductions in N_2O emissions from nitrification inhibitors (NI) are substantial, but remain uncertain because measurements of N_2O emissions are highly variable and discontinuous. Mathematical modelling may offer an opportunity to estimate these reductions if the processes causing variability in N_2O emissions can be accurately simulated. In this study, the effect of NI was simulated with a simple, time-dependent algorithm to slow NH_4^+ oxidation in the ecosystem model *ecosys*. Slower nitrification modelled with NI caused increases in soil NH_4^+ concentrations and reductions in soil NO_3^- concentrations and in N_2O fluxes that were consistent with those measured following fall and spring applications of slurry over two years from 2014 to 2016. The model was then used to estimate direct and indirect effects of NI on seasonal and annual emissions. After spring slurry applications, NI reduced N_2O emissions modelled and measured during the drier spring of 2015 (35% and 45%) less than during the wetter spring of 2016 (53% and 72%). After fall slurry applications, NI reduced modelled N_2O emissions by 58% and 56% during late fall in 2014 and 2015, and by 8% and 33% during subsequent spring thaw in 2015 and 2016. Modelled reductions were consistent with those from meta-analyses of other NI studies. Simulated NI activity declined over time, so that reductions in N_2O emissions modelled with NI at an annual time scale were relatively smaller than those during emission events. These reductions were accompanied by increases in NH_3 emissions and reductions in NO_3^- losses with NI that caused changes in indirect N_2O emissions. With further parameter evaluation, the addition of this algorithm for NI to *ecosys* may allow emission factors for different NI products to be derived from annual N_2O emissions modelled under diverse site, soil, land use and weather.

28

1. INTRODUCTION

30   Nitrification inhibitors (NI) have frequently been found to reduce N_2O emissions from

31 fertilizer and slurry applications in agricultural fields. In a meta-analysis of field experiments

32 conducted to 2008, Akiyama et al. (2010) found average reductions of $38 \pm 6\%$ in N_2O emissions

33 from NI with some variation attributed to land use type and emission rates. Similar average

34 reductions of 35 - 40% were reported in more recent meta-analyses by Ruser and Schulz (2015),

35 Gilsanz et al. (2016) and Gao and Bian (2017). However the magnitudes of these reductions are

36 uncertain because they vary with rate and timing of fertilizer or slurry application, with land use

37 and ecosystem type (Aikyama et al., 2010) and with application method (Zhu et al., 2016).

38 These magnitudes are also uncertain because measurements of the N_2O emissions on which they

39 are based are highly variable temporally and spatially, and difficult to sustain over the annual

40 time periods needed to estimate NI reductions.

41   The effects of NI on N_2O emissions are attributed to inhibition of ammonia

42 monooxygenase which slows the oxidation of NH_4^+ to NO_2^- during nitrification (Subbarao et al.,

43 2006), and hence slows the reduction of NO_2^- to N_2O during nitrifier denitrification. The

44 consequent slowing of NO_2^- oxidation to NO_3^- would also slow the reduction of NO_3^- to N_2O

45 during denitrification. The effectiveness of NI has been found to decline over time due to

46 mineralization, adsorption and volatilization, depending on NI formulation. The rate of this

47 decline varies among NI products and soil types, and increases with soil temperature (Guardia et

48 al., 2018).

49   The great majority of the studies included in meta-analyses of NI effects on N_2O

50 emissions were conducted following fertilizer or slurry application on warm soils in spring or

51 summer. The effectiveness of NIs with fall applications of fertilizer or slurry on cold soils has

52 thus far received very limited attention (Ruser and Schulz, 2015), although in cold climates N_2O

53 emissions during the spring thaw following fall applications may exceed those during later

54 spring and summer following spring applications (Lin et al., 2018). Emissions during spring

55 thaw were attributed by Wagner-Riddle and Thurtell (1998) to soil NO_3–N concentrations

56 exceeding 20 mg kg^{-1} generated by fall-applied slurry that contributed to total N_2O emissions

3

57   exceeding 0.2 g N m^{-2} measured between January and April of the following year. Large N_2O

58   emissions measured in late winter were attributed by Dungan et al. (2017) to labile N not used by

59   soil microorganisms during the previous fall and winter that was actively metabolized when the

60   soils began to warm in early March. Interannual differences in spring thaw emission events after

61   fall slurry applications were related by Kariyapperuma et al. (2012) to those in total soil mineral

62   N content in the upper 15 cm of the soil profile during spring thaw. The effects of NI on N_2O

63   emissions during spring thaw will therefore depend on the persistence with which NI reduces

64   nitrification in cold soils during fall and winter, and thereby alters mineral N concentrations

65   during the following spring.

66   Reductions in N_2O emissions directly caused by slower nitrification with NI may be

67   partially offset by increases in indirect N_2O emissions from increasing NH_3 emissions caused by

68   greater soil NH_4^+ concentrations (Lam et al., 2017, Qiao et al., 2015). NI may also decrease

69   indirect N_2O emissions by reducing NO_3^- concentrations and hence leaching. Both direct and

70   indirect effects of NI on N_2O emissions must be considered when estimating effects of NI on

71   total N_2O emissions.

72   IPCC Tier 3 methodology for estimating N_2O emissions under diverse climates, soils,

73   fertilizers and land uses includes the use of comprehensive, process-based mathematical models

74   of terrestrial C, N, water and energy cycling (IPCC, 2019). Although NI effects on nitrification

75   have been added to some existing process models (Cui et al., 2014; Del Grosso et al., 2009),

76   testing of modelled NI effects on N_2O emissions against measurements remains limited to brief

77   periods following soil N amendments (e.g. Giltrap et al., 2011). The mathematical model *ecosys*

78   explicitly represents the key processes in nitrification (Grant, 1994), denitrification (Grant, 1991)

79   and associated N_2O emissions (Grant, 1995), and has been tested against measurements of N_2O

80   emissions using micrometeorological methods, and manual and automated chambers (Grant and

81   Pattey, 1999, 2008; Grant et al., 2006, 2016; Metivier et al., 2009). In this study, we propose that

82   applying a time-dependent reduction of NH_4^+ oxidation rates during nitrification will enable

83   *ecosys* to simulate the time course of reductions in N_2O emissions with NI measured after fall

84   and spring applications of dairy slurry in a field experiment. The model is then used to estimate

85   the direct and indirect effects of NI on annual N_2O emissions with fall and spring slurry

86   applications as required for IPCC Tier 3 methodology, and how these effects would change with

87   alternative tillage practices and timings of slurry application.

88

89   **2. MODEL DEVELOPMENT**

90

91   **2.1.General Overview**

92   The hypotheses for oxidation-reduction reactions involving N_2O, and the aqueous and

93   gaseous transport of their substrates and products, are represented in Fig. 1 and described in

94   further detail below. References to equations and definitions listed in Supplements S1, S3, S4, S5

95   and S8 of the Supporting Information (Table 1) are provided for those interested in model

96   methodology, but are not needed for a general understanding of model behaviour. These

97   hypotheses function within a comprehensive model of soil C, N and P transformations, coupled

98   to one of soil water, heat and solute transport in surface litter and soil layers, which are in turn

99   components of the comprehensive ecosystem model *ecosys*.

100

101   **2.2.Mineralization and Immobilization of Ammonium by Microbial Functional Types**

102   Heterotrophic microbial functional types (MFTs) *m* (obligately aerobic bacteria,

103   obligately aerobic fungi, facultatively anaerobic denitrifiers, anaerobic fermenters, acetotrophic

104   methanogens, and obligately aerobic and anaerobic non-symbiotic diazotrophs) are associated

105   with each organic substrate *i* (*i* = manure, coarse woody plant residue, fine non-woody plant

106   residue, particulate organic matter, or humus). Autotrophic MFTs *n* (aerobic NH_4^+ and NO_2^-

107   oxidizers, aerobic methanotrophs and hydrogenotrophic methanogens) are associated with

108   inorganic substrates. These MFTs grow [A25] with energy generated from oxidation of dissolved

109   organic C (DOC) by heterotrophs [H2, H10], of acetate by acetotrophic methanogens, of mineral

110   N (NH_4^+ and NO_2^-) [H11, H15] by nitrifiers, of CH_4 by methanotrophs [G7], or of H_2 by

111   hydrogenotrophic methanogens [G12], coupled with reduction of e$^-$ acceptors O_2 [H4, G22],

112   acetate [G8], NO_x [H7 – H9], and CO_2 [G13].   These MFTs decay according to first-order rate

113   constants [A23] with internal recycling of resources (C, N, P) from structural to nonstructural

114   components *j* (*j* = labile, recalcitrant, nonstructural) varying with nonstructural C:N:P ratios

115   [A24], the decay products of which form humus C, N and P [A35, A36]. Each MFT seeks to

116   maintain a set nonstructural C:N:P ratio by mineralizing NH_4^+ and H_2PO4^- [H1a] from, or by

117   immobilizing NH_4^+, NO_3^- and H_2PO4^- [H1b, H1c] into, its nonstructural N and P components.

118   These transformations control the exchange of N and P between organic and inorganic states,

119   and of O_2 between aqueous and gaseous states, and hence affect the availability of substrates and

120   e^- acceptors for nitrification and denitrification.

121

122   **2.3. Oxidation of DOC and Reduction of Oxygen by Heterotrophs**

123   N_2O is generated when demand for e^- acceptors from oxidation by aerobic heterotrophs

124   and autotrophs (Sec. 2.2) exceeds supply from O_2, requiring explicit modelling of O_2 transport

125   and uptake, and consequent O_2 constraints to oxidation-reduction reactions (Sec. 2.11 below).

126   Constraints on heterotrophic oxidation of DOC imposed by O_2 uptake are solved in four steps:

127   1) DOC oxidation by heterotrophs under non-limiting O_2 is calculated from specific oxidation

128   rates multiplied by active biomasses and an Arrhenius function of T_s, constrained by DOC

129   concentration [H2],

130   2) O_2 reduction to H_2O under non-limiting O_2 (O_2 demand) by aerobic heterotrophs is calculated

131   from step 1 using a set respiratory quotient [H3],

132   3) O_2 reduction to H_2O under ambient O_2 is calculated from radial O_2 diffusion through water

133   films with thicknesses determined by soil water potential [H4a] coupled with active uptake at

134   heterotroph surfaces driven by step 2 [H4b]. O_2 diffusion and active uptake are calculated for

135   each heterotrophic population associated with each organic substrate, allowing [H4] to

136   calculate lower O_2 concentrations at microbial surfaces (O_{2m}) associated with more

137   biologically active substrates (e.g. manure, litter). Localized zones of low O_2 concentration

138   (hotspots) are thereby simulated when O_2 uptake by any aerobic MFT is constrained by O_2

139   diffusion to that functional type. O_2 uptake by each heterotrophic MFT is affected by

140   competition for O_2 uptake with other heterotrophs, nitrifiers, roots and mycorrhizae,

141   calculated from its biological O_2 demand relative to those of other aerobic functional types.

142   4) DOC oxidation to CO_2 under ambient O_2 is calculated from steps 2 and 3 [H5]. The energy

143   yield of DOC oxidation with O_2 reduction drives the uptake of additional DOC for

144   construction of microbial biomass $M_{i,h}$ according to construction energy costs of each

145   heterotrophic functional type [A21]. Energy costs of denitrifiers are slightly larger than those

6

146   of obligately aerobic heterotrophs, placing denitrifiers at a small competitive disadvantage for

147   growth and hence DOC oxidation under non-limiting O_2.

148

149   **2.4. Oxidation of DOC and Reduction of Nitrate, Nitrite and Nitrous Oxide by**

150   **Denitrifiers**

151   N_2O may be both product and substrate of NO_x reduction coupled with DOC oxidation by

152   denitrifiers. Constraints imposed by NO_3^- availability on denitrifier DOC oxidation are solved

153   in five steps:

154   1) NO_3^- reduction to NO_2^- by heterotrophic denitrifiers under non-limiting NO_3^- is calculated

155   from demand for e^- acceptors by denitrifiers for DOC oxidation to CO_2, but not met from O_2

156   reduction to H_2O because of diffusion limitations to O_2 supply (Sec. 2.3 step 3). This unmet

157   demand is transferred to NO_3^- [H6],

158   2) NO_3^- reduction to NO_2^- under ambient NO_3^- is calculated from step 1, accounting for relative

159   concentrations and affinities of NO_3^- and NO_2^- [H7],

160   3) NO_2^- reduction to N_2O under ambient NO_2^- is calculated from demand for e^- acceptors not met

161   by NO_3^- reduction in step 2, accounting for relative concentrations and affinities of NO_2^- and

162   N_2O. This unmet demand is transferred to NO_2^- [H8].

163   4) N_2O reduction to N_2 under ambient N_2O is calculated from demand for e^- acceptors not met by

164   NO_2^- reduction in step 3, and hence transferred to N_2O [H9].

165   5) additional energy yield from DOC oxidation to CO_2 enabled by NO_x reduction in steps 2, 3

166   and 4 is added to that enabled by O_2 reduction from [H5], which drives additional DOC

167   uptake for construction of $M_{i,n}$. This additional uptake offsets the disadvantage incurred by the

168   larger construction energy costs of denitrifiers (Sec. 2.3 step 4).

169

170   **2.5. Oxidation of Ammonium and Reduction of Oxygen by Nitrifiers**

171   N_2O may also be generated by reduction of NO_2^- coupled with oxidation of NH_4^+ by

172   autotrophic nitrifiers. Constraints on nitrifier oxidation of NH_4^+ imposed by O_2 uptake are solved

173   in four steps:

174   1) Oxidation of NH_4^+ (in dynamic equilibrium with NH_3 [E24]) under non-limiting O_2 is

175   calculated from a specific oxidation rate multiplied by active biomass and an Arrhenius

176   function of T_s, and constrained by NH_4^+ and CO_2 concentrations [H11],

177   2) O_2 reduction to H_2O under non-limiting O_2 (O_2 demand) is calculated from step 1 using set

178   respiratory quotients [H12],

179   3) O_2 reduction to H_2O under ambient O_2 is calculated from radial O_2 diffusion through water

180   films of thickness determined by soil water potential [H13a] coupled with active uptake at

181   nitrifier surfaces driven by step 2 [H13b]. O_2 uptake by nitrifiers is affected by competition

182   for O_2 uptake with heterotrophic DOC oxidizers, roots and mycorrhizae, calculated from its

183   biological O_2 demand relative to those of other aerobic functional types.

184   4) NH_4^+ oxidation to NO_2- under ambient O_2 is calculated from steps 2 and 3 [H14]. The energy

185   yield of NH_4^+ oxidation drives the fixation of CO_2 for construction of microbial biomass $M_{i,n}$

186   according to nitrifier construction energy costs.

187

188   **2.6. Oxidation of Nitrite and Reduction of Oxygen by Nitrifiers**

189   Constraints on nitrifier oxidation of NO_2^- to NO_3^- imposed by O_2 uptake [H15 - H18] are

190   solved in the same way as are those of NH_4^+ to NO_2^- [H11 - H14]. The energy yield of NO_2^-

191   oxidation drives the fixation of CO_2 for construction of microbial biomass $M_{i,o}$ according to

192   nitrifier construction energy costs.

193

194   **2.7. Oxidation of Ammonium and Reduction of Nitrite by Nitrifiers**

195   In both nitrifier and denitrifier processes, N_2O is generated from reduction of NO_2^-, the

196   availability of which is controlled by NO_2^- oxidation (Sec. 2.6). Under low O_2 concentrations

197   NO_2^- oxidation is suppressed [H18], favoring NO_2^- reduction. Constraints on nitrifier oxidation

198   of NH_4^+ imposed by NO_2^- availability are solved in three steps:

199   1) NO_2^- reduction to N_2O under non-limiting NO_2^- is calculated from e^- acceptors demanded by

200   NH_4^+ oxidation to NO_2^- but not met by O_2 for reduction to H_2O because of diffusion

201   limitations to O_2 supply, and hence transferred to NO_2^- [H19],

202   2) NO_2^- reduction to N_2O under ambient NO_2^- and CO_2 is calculated from step 1 [H20],

203   competing for NO_2^- with denitrifiers [H8] and nitrifiers [H18],

204   3) energy yield from additional NH_4^+ oxidation to NO_2^- enabled by NO_2^- reduction in step 2

205   [H21] is added to that enabled by O_2 reduction from Sec. 2.5 step 4 [H14] which drives the

206   fixation of additional CO_2 for construction of $M_{i,n}$.

207

208 **2.8. Uptake of Ammonium and Reduction of Oxygen by Roots and Mycorrhizae**

209   NH_4^+ oxidation and O_2 reduction by nitrifiers compete for substrates with NH_4^+ uptake

210 and O_2 reduction by other MFTs, and by roots and mycorrhizae.

211 1) NH_4^+ uptake by roots and mycorrhizae under non-limiting O_2 is calculated from mass flow

212   and radial diffusion between adjacent roots and mycorrhizae [C23a] coupled with active

213   uptake at root and mycorrhizal surfaces [C23b]. Active uptake is subject to product inhibition

214   by root nonstructural N:C ratios [C23g] where nonstructural N is the active uptake product,

215   and nonstructural C is the CO_2 fixation product transferred to roots and mycorrhizae from the

216   canopy.

217 2) O_2 reduction to H_2O under non-limiting O_2 is calculated from O_2 demands for NH_4^+ uptake in

218   step 1, and for oxidation of root and mycorrhizal nonstructural C for root maintenance and

219   growth using a set respiratory quotient [C14e],

220 3) O_2 reduction to H_2O under ambient O_2 is calculated from mass flow and radial diffusion

221   between adjacent roots and mycorrhizae [C14d] coupled with active uptake at root and

222   mycorrhizal surfaces driven by step 2 [C14c]. O_2 uptake by roots and mycorrhizae is also

223   affected by competition with O_2 uptake by heterotrophic DOC oxidizers, and autotrophic

224   nitrifiers, calculated from their biological O_2 demands relative to those of other populations.

225 4) oxidation of root and mycorrhizal nonstructural C to CO_2 under ambient O_2 is calculated from

226   steps 2 and 3 [C14b],

227 5) NH_4^+ uptake by roots and mycorrhizae under ambient O_2 is calculated from steps 1, 2, 3 and 4

228   [C23b].

229

230 **2.9. Nitrification Inhibition**

231   For this study, NIs were assumed to reduce specific rates of NH_4^+ oxidation by nitrifiers

232 in Sec. 2.5 step 1, thereby simulating inhibition of ammonia monooxygenase (Subbarao et al.,

233 2006). This reduction was represented by a time-dependent scalar I:

234

235     $I_{t_l} = I_{t-1_l} - I_{t_l} * R_I * f_{Ts_l}$ [1]

236

237 where t is the current time step (h), t-1 is the previous time step (h), I is the inhibition (initialized

238 to 1.0 at t = 0 at the time of application), R_I is the rate constant for decline of I representing NI

239   degradation (set to 2.0 x 10^{-4} h^{-1} for more persistent NIs such as DMPP and to 1.0 x 10^{-3} h^{-1} for

240   less persistent NIs such as nitrapyrin (Ruser and Schulz, 2015)), f_{Ts} is an Arrhenius function of

241   soil temperature (T_s) used to simulate T_s effects on microbial activity (Sec. 2.3 step 1), and l is

242   the soil layer in which NI is present. The values of R_I and f_{Ts} for DMPP were selected to give

243   time and temperature dependencies of DMPP activity following application inferred from

244   incubation studies by Guardia et al. (2018). Model results for NI presented below are those using

245   the smaller R_I for DMPP unless stated as those using the larger R_I for nitrapyrin.

246

247   Specific rates of NH_4^+ oxidation (Sec. 2.5 step 1) with NI was calculated as:

248

249        $X'_{NH4t_l} = X''_{NH4_l} * (1.0 - I_{t_l} / (1.0 + [NH_4^+]_l / K_{iNH4}))$ [2]

250

251   where X'_{NH4} and X''_{NH4} are specific NH_4^+ oxidation rates with and without NI (g N g nitrifier C^{-1}

252   h^{-1}), $[NH_4^+]$ is the aqueous NH_4^+ concentration (g N m^{-3} in dynamic equilibrium with $[NH_3]$), and

253   K_{iNH4} is an inhibition constant set at 7000 g N m^{-3} to reduce inhibition at very large $[NH_4^+]$ as

254   suggested in Janke et al. (2019). These rates were used to calculate nitrification rates [H11]:

255

256        $X_{NH4t_l} = X'_{NH4t_l} M_{n_l} f_{t_l} \{[NH_4^+]_l / ([NH_4^+]_l + K_{NH4})\} \{[CO_{2}s]_l / ([CO_{2}s]_l + K_{CO2})\}$ [3]

257

258   where X_{NH4t} is the nitrification rate (g N m^{-2} h^{-1}), M_n is the nitrifier biomass (g C m^{-2}) and K_{NH4}

259   and K_{CO2} are half-saturation constants for aqueous NH_4^+ and CO_2 (g N and C m^{-3}). NI in Eq. 1

260   slows X'_{NH4t} in Eq. 2 and thereby X_{NH4t} in Eq. 3, and hence slows NO_2^- production from

261   nitrification (Sec. 2.5 step 4), and thereby N_2O production from nitrification (Sec. 2.7 step 2) and

262   denitrification (Sec. 2.4 step 3). By slowing X_{NH4t} in Eq. 3, NI also reduces nitrification energy

263   yield and hence M_n growth, biomass [A25] and O_2 uptake [H13], thereby further reducing N_2O

264   production.

265

266   **2.10.   Cation Exchange and Ion Pairing of Ammonium**

267   Availability of NH_4^+ to nitrifiers is also controlled by NH_4^+ adsorption. A Gapon

268   selectivity coefficient is used to solve cation exchange of NH_4^+ vs. Ca^{2+} [E10] as affected by

269   other cations [E11] – [E15] and CEC [E16]. A solubility product is used to equilibrate soluble

10

270   NH_4^+ and NH_3 [E24] as affected by pH [E25] and other solutes [E26 – E57]. Equilibrium NH_4^+

271   concentrations drive NH_4^+ oxidation (Sec. 2.5 step 1) and NH_3 volatilization (Sec. 2.11 below).

272

273   **2.11.   Soil Transport and Surface - Atmosphere Exchange of Aqueous and Gaseous**

274   **Substrates and Products**

275   O_2 uptake and N_2O emissions in Sec. 2.3 to 2.8 above are governed by aqueous and

276   gaseous transport processes in vertical and lateral directions:

277   1) Exchanges of all modelled gases γ (γ = O_2, CO_2, CH_4, N_2, N_2O, NH_3 and H_2) between

278   aqueous and gaseous states within each soil layer are driven by disequilibrium between

279   aqueous and gaseous concentrations according to a T_s-dependent solubility coefficient,

280   constrained by an interphase transfer coefficient based on air-water interfacial area that

281   depends on air-filled porosity (θ_g) [D14 – D15] (Fig. 1).

282   2)   These gases undergo vertical and lateral convective-dispersive transport through soil in

283   gaseous [D16] and aqueous [D19] states driven by soil water flux and by gas concentration

284   gradients. Dispersive transport is controlled by gaseous diffusion [D17] and aqueous

285   dispersion [D20] coefficients calculated from θ_g and water-filled porosity (θ_w). Both θ_g and

286   θ_w are affected by ice-filled porosity (θ_i) from freezing and thawing driven by soil heat fluxes

287   [D13].

288   3) Vertical exchanges of all gases between the atmosphere and both gaseous and aqueous states

289   at the soil surface are driven by atmosphere - surface gas concentration differences and by

290   boundary layer conductance above the soil surface, calculated from wind speed and from

291   vegetation density and surface litter [D15]. These exchanges give modelled surface fluxes

292   used in tests against surface fluxes measured in field experiments.

293   4) All solutes can be lost/gained by lateral surface runoff/runon modelled from Manning's

294   equation [D1a] with surface water depth [D2] calculated from surface water balance [D4]

295   using kinematic wave theory, and by lateral subsurface discharge/recharge modelled from

296   convective exchange through subsurface boundaries with an external water table.

297

298   **3. FIELD EXPERIMENT**

299

3.1. Site Description and Experimental Design

An experiment was established on a Black Chernozem (Table 2) under barley silage from 2014 to 2016 at the South Campus Farm in Edmonton, AB, Canada (53°29'30"N, 113°31'53"W), using an incomplete split-plot design (main plot: fall vs. spring application of dairy slurry; split plot: control vs. NI treatments) with three replicates (Lin et al., 2018). The NI products ENTEC (Eurochem Agro, Mannheim, Germany) and eNtrench Nitrogen Stabilizer (Dow Chemical Company, Dow AgroSciences, Calgary, AB, Canada) were mixed with the slurry immediately before application to provide 0.4 kg ha^{-1} active ingredient with slurry injection of 56.17 m^3 ha^{-1} at 12.7 to 15.2 cm (average 14 cm) depth and 28 cm spacing. Measured concentrations of NH_4^+ and of organic N and C in each slurry application were used to calculate rates of NH_4^+, organic N and organic C amendments (Table 3). Soil NH_4^+ concentrations were measured from 0 to 10 cm every 2 – 3 weeks between spring thaw and autumn freezing in 2014, 2015 and 2016.

Weather data (radiation, air temperature (T_a), humidity, windspeed and precipitation) were recorded hourly from 2012 through 2016 at the South Campus Farm. During the first experimental year (16 Sep. 2014 to 15 Sep. 2015) T_a remained 1 – 2 ^{o}C higher than historical (1981 – 2010) averages (Lin et al., 2018) (Table 4). Precipitation was slightly higher than historical averages during autumn and winter, but was about one-half those during spring and summer. During the second experimental year (16 Sep. 2015 to 15 Sep. 2016), T_a was higher than that of the first year during winter and early spring, and similar during late spring and summer. However precipitation during the second year was lower from autumn to early spring and much higher during late spring and summer.

3.2. N$_2$O Flux Measurements

N$_2$O fluxes were measured from as soon as possible after spring thaw to late summer during both experimental years with automated chambers (height 26 cm, area 0.216 m^2) connected by 0.5 cm i.d. tubes to a FTIR gas analyzer (GASMET model CX4025, Temet Instruments, Finland) through which air flow was maintained at 5.1 L min^{-1}. During each 20 minute measurement period, the chambers remained open for the first 5 minutes to restore ambient N$_2$O concentrations in the gas analyzer, after which chambers were closed and N$_2$O concentrations were measured at 10 Hz and averages recorded at 1 minute intervals. Concentrations during the

Biogeosciences
Discussions
Open Access
EGU

331 first minute after closure were discarded and those during the following 14 minutes were used to

332 calculate fluxes using linear regression with an acceptance criterion of $R^2 \geq 0.85$. Based on the

333 analytical precision of the gas analyzer, the N_2O flux detection limit was determined to be +/-

334 0.03 mg N m^{-2} h^{-1}.

335

336 N_2O emissions were also measured once or twice per week from spring thaw to autumn

337 freezing during both experimental years with manually operated chambers as described in Lin et

338 al. (2018). The time required for installation of the automated chambers after snowmelt limited

339 their ability to measure N_2O emissions during spring thaw, so that measurements from the

340 manually operated chambers were used to evaluate emissions during these periods.

341

342 ## 4. MODEL EXPERIMENT

343

344 ### 4.1. Model Spinup

345 To simulate site conditions prior to the experiment, *ecosys* was initialized with the properties

346 of the Black Chernozem (Table 2) and run from model dates 1 Jan. 1992 to 31 Dec. 2013 under

347 a repeating 5-year sequence of weather data (radiation, air temperature (T_a), humidity,

348 windspeed and precipitation recorded hourly from 2012 through 2016 at the South Campus

349 Farm. During each year of the spinup run, barley was planted, fertilized and harvested as silage

350 to reproduce land use practices reported from the field site.

351

352 ### 4.2. Model Runs

353 The spinup run was extended from 1 Jan. 2014 to 31 Dec. 2016 under weather data recorded

354 from 2014 to 2016 with the land use schedules and practices from the field site (Table 3). Each

355 modelled slurry application was added to the soil layer the depth of which corresponded to that

356 of slurry injection in the field experiment (14 cm). Modelled applications were accompanied by

357 addition of water corresponding to the volume and depth of the application (5.6 mm from 56.17

358 m^3 ha^{-1} at 14 cm in Sec. 3.1), and by tillage using a coefficient for surface litter incorporation

359 and soil mixing of 0.2 to the depth of application, based on field observations. A control run was

360 also conducted in which no slurry applications were modelled. For all silage harvests, cutting

361 height and harvest efficiency were set to 0.15 m and 0.9, so that 0.9 of all plant material above

13

362   0.15 m was removed as yield. Concentrations of NH_4^+ and NO_3^-, and N_2O emissions modelled

363   during key emission events, were compared with measured values (Sec. 3.1 and 3.2), and

364   modelled emissions were then aggregated into seasonal and annual values.

365

366   There is some flexibility in the timing of fall slurry application between crop harvest in late

367   summer and soil freezing in early November. To examine how timing of fall slurry application

368   would affect subsequent N_2O emissions with and without NI, fall slurry application dates were

369   advanced or delayed by 2 weeks from those in Table 3, and effects on spring and annual N_2O

370   emissions were evaluated. To examine how increased tillage during slurry application would

371   affect subsequent N_2O emissions with and without NI, coefficients for surface litter

372   incorporation and soil mixing to the depth of slurry application were raised from 0.2 to 0.5 and

373   0.8 for fall and spring applications.

374

375   **5. RESULTS**

376

377   **5.1. NI and Soil NH_4^+ and NO_3^- Concentrations**

378   **5.1.1.   Fall Slurry Applications**

379   In the model, NI slowed NH_4^+ oxidation (Sec. 2.9, Eq. 3) so that declines in NH_4^+

380   concentrations modelled and measured after fall and spring slurry applications with NI were

381   slower than those without NI (Fig. 2a), particularly during winter when declines in inhibition

382   were slowed by low T_s (Sec. 2.9, Eq. 1) following the onset of soil freezing modelled at the depth

383   of slurry injection (DOY 313 in 2014 and DOY 318 in 2015 in Fig. 2a). Overwinter declines in

384   NH_4^+ concentrations were slower during the winter of 2015/2016 with lower T_s modelled under

385   less winter precipitation and hence shallower snowpack (Table 4). These slower declines caused

386   larger NH_4^+ concentrations to be modelled during the following spring, consistent with

387   measurements (Fig. 2a). The slower declines in NH_4^+ concentrations modelled with NI caused

388   slower rises in NO_3^- concentrations following fall slurry applications (Fig. 2c). However slower

389   rises with NI were not always apparent in the measured NO_3^- concentrations.

390

391   **5.1.2.   Spring Slurry Applications**

14

392   Declines in NH_4^+ concentrations modelled after slurry applications with NI in spring 2015

393   and 2016 were also slower than after those without NI (Fig. 2b), consistent with higher NH_4^+

394   concentrations measured after spring application with DMPP in both years (Fig. 2b). These

395   slower declines caused slower rises in NO_3^- concentrations to be modelled following spring

396   slurry applications with NI (Fig. 2d).

397

398   **5.2. NI and Soil Gas Concentrations**

399   **5.2.1. Fall Slurry Applications**

400   In the model, spring snowmelt and soil thaw raised θ_w and lowered θ_g, slowing gas transfers

401   in gaseous phases and gas exchanges between gaseous and aqueous phases (Sec. 2.11 step 1, 2).

402   Slower O_2 transfers relative to O_2 uptake (Sec. 2.3, 2.5 and 2.6) forced reductions in aqueous O_2

403   concentrations (O_{2s}) to be modelled during early spring in 2015 (Fig. 3a,b) and 2016 (Fig. 3c,d)

404   following fall slurry applications in 2014 and 2015. Declines in O_{2s} were later but more rapid in

405   2015 than in 2016, following greater winter precipitation and hence greater snowmelt in

406   2014/2015 (Table 4). Earlier and more persistent declines in O_{2s} were modelled in 2016 because

407   greater θ_i modelled with less thermal insulation under a shallower snowpack (Sec. 2.11 step 2)

408   reduced or eliminated θ_g during much of the winter. Drainage of meltwater after snowmelt

409   eventually lowered θ_w and raised θ_g, allowing O_{2s} to return to atmospheric equivalent

410   concentrations.

411

412   Declines in O_{2s} in slurry-amended treatments drove increases in aqueous N_2O concentrations

413   (N_2O_s) (Fig. 3b,d) during winter and early spring (Sec. 2.7, step 1). These rises were similar with

414   and without NI, in spite of higher NH_4^+ concentrations without NI (Fig. 2a). Rises in θ_g

415   following spring drainage allowed volatilization of N_2O from aqueous to gaseous phases (Sec.

416   2.11 step 1), reducing N_2O_s and driving N_2O emissions modelled during spring thaw.

417

418   **5.2.2. Spring Slurry Applications**

419   Declines in O_{2s} modelled after spring slurry application were small during the drier spring of

420   2015 (Table 4) (Fig. 3e), but were greater with lower θ_g during the wetter spring of 2016 (Fig.

421   3g) (Sec. 2.11). During both years, these declines were more rapid with slurry than without, but

15

422   less rapid with NI-amended slurry than with unamended slurry. Greater declines in O_{2s} modelled

423   in 2016 vs. 2015 drove greater increases in N_2O_s (Sec. 2.7), particularly without NI, and hence

424   greater emissions of N_2O (Sec. 2.11) during subsequent declines in N_2O_s.

425

426   **5.3. NI and N_2O Fluxes**

427   **5.3.1. Fall Slurry Applications**

428   Smaller rises and subsequent declines in N_2O_s modelled with NI than without (Fig. 3b) drove

429   smaller N_2O emission events modelled during spring thaw in 2015 (Fig. 4a) following slurry

430   application in fall 2014 (Fig. 4b). These events were driven by increases in θ_g during

431   midafternoon thawing of near-surface soil (Sec. 2.11 step 1), but were terminated by loss of θ_g

432   during nighttime refreezing. These events preceded the start of the automated chamber

433   measurements on DOY 102 and so could not be corroborated by them. However measurements

434   with manual chambers earlier in spring 2015 by Lin et al. (2018) indicated that N_2O emission

435   events occurred from DOY 85 to 100 that were similar in magnitude although not always in

436   timing with those modelled (Fig. 4b). These measured emissions were smaller with NI than

437   without, consistent with modelled emissions.

438

439   The smaller rises and subsequent declines in N_2O_s modelled with NI than without in the

440   winter of 2016 (Fig. 3d) drove smaller emission events during thawing and refreezing of near-

441   surface soil in spring 2016 (Fig. 5a) following slurry application in fall 2015 (Fig. 5b). These

442   modelled events preceded the start of automated chamber measurements on DOY 91, but earlier

443   measurements with manual chambers indicated N_2O emission events occurred from DOY 74 to

444   93. The smaller emission events modelled with NI were consistent with those measured using the

445   manual chambers, although some larger emissions measured with DMPP using the automated

446   chambers from DOY 91 to 102 were not modelled (Fig. 5b). In both years, emissions modelled

447   and measured without slurry remained very small, consistent with low N_2O_s (Fig. 3b,f).

448

449   **5.3.2. Spring Slurry Applications**

450   Modelled N_2O emissions closely followed measured values during a brief emission event

451   following slurry application in the drier spring of 2015 (Fig. 6a,b), driven by small rises and

452   declines in N2O$_s$ (Fig. 3f). The smaller rise and decline in N_2O_s modelled with NI than without

453 drove smaller N_2O emissions which declined more rapidly after application than did emissions

454 measured with DMPP (Fig. 6b).

455

456   Emissions modelled without NI in the wetter spring of 2016 were larger than those in the

457 drier spring of 2015 (Fig. 7a,b), driven by a larger rise and decline in N_2O_s with lower θ_g (Fig.

458 3h). These emissions were suppressed by low θ_g with soil wetting during heavy rainfall on DOY

459 141 – 143 shortly after slurry application (Fig. 7a,b), but resumed when θ_g rose with soil

460 drainage thereafter (Fig. 7b). Emissions modelled without NI remained greater than those

461 measured until DOY 150, after which modelled values declined with soil drying while measured

462 value rose (Fig. 7b). Greater reductions in N_2O_s (Fig. 3h) and hence in N_2O emissions were

463 modelled with NI after slurry application in the wetter spring of 2016 (Fig. 7b) than in the drier

464 spring of 2015 (Fig. 6b). In both years, emissions modelled and measured without slurry

465 remained very small, consistent with low N_2O_s (Fig. 3f,h).

466

467   **5.4. NI Effects on Seasonal and Annual N_2O Emissions**

468   **5.4.1. Modelled vs. Measured N_2O Emissions after Spring Slurry Applications**

469   Total N_2O emissions modelled without NI and with R_I for DMPP or nitrapyrin (Sec. 2.9) were

470 compared with those aggregated from automated chamber measurements over 30-day periods

471 after spring slurry applications in 2015 and 2016 (Table 5). Total emissions modelled and

472 measured without NI were greater during the wetter spring of 2016 than during the drier spring

473 of 2015. Reductions in 30 d emissions modelled and measured with R_I for DMPP and nitrapyrin

474 were greater during the wetter spring in 2016 (53% and 41%) than during the drier spring in

475 2015 (35% and 30%). These reductions were somewhat smaller than those measured with DMPP

476 and nitrapyrin in 2016 (72% and 64%) and 2015 (45% and 36%). Emissions were not measured

477 with automated chambers after fall slurry applications, preventing comparisons with modelled

478 values.

479

480   **5.4.2. Seasonal and Annual N_2O Emissions Modelled After Fall and Spring Slurry**

481   **Applications**

482   **5.4.2.1. Fall Slurry Applications**

483   NI greatly reduced N_2O emissions modelled from fall applications during autumn (16 Sep. –

484   31 Dec. in Table 6) in 2014 and 2015, slightly reduced N_2O emissions modelled during the

485   following winter and early spring (1 Jan. – 30 Apr.), but slightly raised N_2O emissions modelled

486   during the following summer (1 May – 15 Sep.) in both 2015 and 2016. Annual emissions

487   modelled with NI were reduced from those without NI by 26% and 38% in 2014/2015 and

488   2015/2016 respectively (Table 6). The reduction modelled in 2014/2015 was similar to one of

489   23% estimated for DMPP from manual chamber measurements from 1 Oct. 2014 to 30 Sep.

490   2015 by Lin et al. (2018), although the reduction with NI modelled in 2015/2016 was greater

491   than one of 15% estimated from manual chamber measurements from 1 Oct. 2015 to 30 Sep.

492   2016.

493

494   **5.4.2.2. Spring Slurry Applications**

495   Reductions in annual N_2O emissions modelled from spring slurry applications with DMPP

496   and nitrapyrin occurred almost entirely during late spring and summer (1 May – 15 Sep. in Table

497   6). These reductions were 22% and 40% from those modelled without NI in 2014/2015 and

498   2015/2016 respectively (Table 6). The reduction modelled with NI in 2014/2015 was greater

499   than one of 0% for DMPP estimated from manual chamber measurements from 1 Oct. 2014 to

500   30 Sep. 2015 by Lin et al. (2018), although the reduction modelled in 2015/2016 was similar to

501   one of 38% estimated from manual chamber measurements from 1 Oct. 2015 to 30 Sep. 2016.

502

503   **5.5. Effects of Management on Seasonal and Annual N_2O Emissions Modelled After**

504   **Fall and Spring Slurry Applications**

505   Advancing fall slurry application by 2 weeks increased N_2O emissions modelled with and

506   without NI during autumn but reduced those during subsequent spring thaw (F -2 in Table 6) so

507   that annual emissions modelled with and without NI were similar to those in F with the

508   application dates in the experiment (Table 3). Delaying fall slurry application by 2 weeks

509   reduced N_2O emissions modelled with and without NI only slightly during autumn, but greatly

510   increased emissions modelled during subsequent spring thaw (F +2 in Table 6), particularly with

511   the later fall application in 2016 (Table 3). Consequently delaying fall slurry application by 2

512   weeks caused substantial increases in annual N_2O emissions. However reductions in N_2O

513   emissions modelled with NI in F +2 in 2015 and 2016 (34% and 47%) were greater than those in

18

514   F (26% and 38%), because inhibition declined more slowly in colder soil (Eq. 1), particularly

515   with later application in 2016.

516

517   Increasing surface litter incorporation and soil mixing during fall slurry application raised

518   N_2O emissions modelled without NI only slightly during 2014/2015, but substantially during

519   2015/2016, particularly during spring thaw (F 0.5 and F 0.8 vs. F in Table 6). Increasing surface

520   litter incorporation and soil mixing during spring slurry application had limited effects on

521   emissions (S 0.5 and S 0.8 vs. S in Table 6). Greater mixing caused reductions in N_2O emissions

522   modelled with NI to be smaller relative to those without NI.

523

524   **5.6. NI Effects on Annual Mineral N Losses and NH₃ Emissions**

525   Injecting the slurry to 14 cm in the model suppressed NH_3 emissions with limited soil mixing,

526   and caused only very small emissions with greater mixing (Table 7). Higher NH_4^+ concentrations

527   modelled with NI (Fig. 2a,b) increased net NH_3 emission, particularly if fall slurry application

528   was delayed or soil mixing was increased in 2014/2015.

529

530   The subhumid climate at Edmonton (Table 4) caused modelled NO_3^- losses to remain small.

531   For both fall and spring applications, lower NO_3^- concentrations modelled with NI (Fig. 2c,d)

532   caused small reductions in NO_3^- losses.

533

534   **5.7. NI Effects on Barley Silage Yields**

535   Silage yields modelled with fall slurry application were smaller than those measured in

536   the drier year 2015, but those modelled with both applications were greater than those measured

537   in the wetter year 2016, likely because of lodging observed in the field plots following the

538   second year of heavy manure use (Table 8). Modelled yields were unaffected by NI for fall and

539   spring applications in both years, although measured yields were raised by NI with spring

540   application in 2015. Modelled yields were affected by the cutting height and harvest efficiency

541   set in the model runs (Sec. 4.2).

542

543   **6. DISCUSSION**

544   **6.1. Process Modelling of N_2O Emissions**

19

545   N$_2$O emissions were driven by declines in O$_{2g}$ and O$_{2s}$ modelled by equilibrating O$_2$ active

546   uptake by autotrophic and heterotrophic oxidation (Sec. 2.5 step 3 and Sec. 2.3 step 3) with O$_2$

547   diffusion and dissolution through gaseous and aqueous phases, and dissolution from gaseous to

548   aqueous phases, largely controlled by θ_g (Sec. 2.11 steps 1 - 3). These O$_2$ transfers were

549   sustained by concentration gradients from O$_{2g}$ to O$_{2s}$ and from O$_{2s}$ to O$_{2m}$, so that declines in O$_{2s}$

550   (Fig. 3) and O$_{2m}$ were relatively larger than those in O$_{2g}$. These greater declines enabled N$_2$O

551   emissions to be modelled from O$_2$ deficits while O$_{2g}$ remained above one-half of atmospheric

552   concentration, consistent with observations of O$_{2g}$ during N$_2$O emissions from incubation and

553   field experiments (Nguyen et al., 2017; Owens et al., 2017). These O$_2$ deficits were modelled

554   using a K_m for O$_{2m}$ of 10 μM by nitrifiers (Sec. 2.5 step 3) and 2 μM by denitrifiers (Sec. 2.3 step

555   3) derived from biochemical studies by Focht and Verstraete (1977). These K_m are less than 5%

556   and 1% of atmospheric equivalent concentration, indicating the importance of explicitly

557   simulating gaseous and aqueous transport processes (Sec. 2.11) when modelling N$_2$O emissions.

558

559   O$_2$ deficits were modelled in spring thaw 2015 (Fig. 3a), when diffusion was sharply reduced

560   by soil saturation because drainage from snowmelt and soil thaw was impeded by underlying ice

561   layers. These declines drove N$_2$O generation (Fig. 3b) and emission (Fig. 4b) almost entirely

562   from NO$_2^-$ reduced during spring thaw. O$_2$ deficits were also modelled during winter 2016 when

563   increased θ_l from soil freezing with lower T_s under a shallower snowpack caused near-surface

564   soil porosity to be fully occupied by ice and water. Consequent loss of θ_g greatly reduced

565   surface gas exchange (Sec. 2.11) and hence gradually reduced soil O$_2$ concentrations,

566   particularly with increased O$_2$ demand from fall slurry application (Fig. 3c). The extended period

567   of low O$_{2s}$ prolonged overwinter accumulation of N$_2$O$_s$ after fall slurry application (Fig. 3d).

568   Transient increases in θ_g during soil freeze-thaw cycles caused several N$_2$O emission events to

569   be modelled during spring thaw in 2016, mostly from degassing through volatilization of

570   overwinter N$_2$O$_s$ (Fig. 5b) (Sec. 2.11 step 1). Degassing events in the model were consistent with

571   field observations by Chantigny et al. (2017) that passive degassing of accumulated gases made a

572   significant contribution to spring thaw emissions during which two or more consecutive emission

573   peaks were often observed. In the model, the contribution by degassing of overwinter N$_2$O$_s$ to

574   spring thaw emissions increased with intensity and duration of soil freezing during the previous

575   winter. N$_2$O emissions simulated during spring thaw were thus driven by concurrent NO$_2^-$

576   reduction during spring thaw (2015) and by earlier NO_2^- reduction accumulated over the

577   previous winter (2015/2016), as has been proposed from experimental observations (Teepe et al.,

578   2004).

579

580   O_2 deficits were also caused by rapid increases in O_2 active uptake with addition of labile C

581   in slurry, the rapid decomposition and oxidation of which (Sec. 2.3 step 1) caused transient

582   declines in O_{2s} with soil wetting from slurry application and precipitation (Fig. 3e,g). After slurry

583   application in the wetter spring of 2016, modelled O_{2g} declined to *ca*. one-half of atmospheric

584   concentration, driving the sharp declines in O_{2s} shown in Fig. 3g. The modelled declines in O_{2g}

585   were consistent with results from an incubation of wetted soil amended with cattle slurry by

586   Nguyen et al. (2017) in which O_{2g} declined below one-half of atmospheric concentration within

587   one day of slurry application and gradually rose again after two days, while no decline occurred

588   in an unamended soil. The period of low O_{2s} in this incubation study co-incided with peak

589   emissions of CO_2 and N_2O from the amended soil, as was modelled here in Fig. 3f,h and Fig. 6b

590   and 7b. This co-incidence indicated that NH_4^+ and DOC oxidation drove O_2 deficits from

591   demand for O_2 from oxidation vs. supply of O_2 through convection – dispersion, which caused

592   NO_2^- reduction as represented in the model, again demonstrating the importance of simulating

593   aqueous and gaseous O_2 transfers when modelling N_2O emissions.

594

595   **6.2. Process Modelling of NI Effects on N_2O Emissions**

596   **6.2.1. Fall Slurry Application**

597   NH_4^+ oxidation in the model (Sec. 2.5 step 4) proceeded rapidly after fall slurry application

598   without NI as indicated by rapid declines in NH_4^+ (Fig. 2a), consistent with observations in other

599   studies that soil NH_4^+ concentrations returned to background levels 30 d after fall slurry

600   application (Rochette et al., 2004). Slower NH_4^+ oxidation modelled with NI (Eq. 3) during fall

601   caused slower declines of soil NH_4^+ before and during freezing and hence larger NH_4^+

602   concentrations during spring thaw (Fig. 2a). These slower declines were modelled from slower

603   decline of I_t with low f_{Ts} in cold soils (Eq. 1) which slowed NH_4^+ oxidation and thereby reduced

604   N_2O emissions simulated during late autumn and spring thaw (Figs. 4b and 5b), despite increased

605   NH_4^+ concentrations (Fig. 3). These reductions were consistent with those from chamber

606   measurements at the Edmonton South Farm (Lin et al., 2017), and with those from a limited

607   number of studies elsewhere in which persistent effects of NI in reducing overwinter N_2O

608   emissions have been found (e.g. Pfab et al., 2012), indicating the importance of f_{Ts} in Eq. 1.

609

610   The slower decline of I_t from low f_{Ts} enabled *ecosys* to simulate larger reductions in N_2O

611   emissions with NI after fall slurry applications in cooler soil vs. spring slurry applications in

612   warmer soil during both years (F during autumn *vs*. S during late spring-summer in Table 6).

613   Reductions in N_2O emissions modelled with NI after fall slurry applications became greater

614   when fall applications were delayed (F +2 in Table 6), further reducing T_s and f_{Ts} during

615   subsequent nitrification. The greater reductions modelled with fall applications were consistent

616   with experimental observations by Merino et al. (2005) who attributed larger reductions in N_2O

617   emissions measured with NI from fall- vs. spring-applied cattle slurry to slower NI degradation

618   in cooler soil. These modelled and experimental results indicated that NI effectiveness in

619   reducing N_2O emissions varies with the effect of fall slurry timing on f_{Ts}.

620

621   The greater reductions in N_2O emissions modelled from delayed fall applications with NI

622   were associated with much greater N_2O emissions modelled from delayed fall applications

623   without NI (F+2 in Table 6). These greater emissions were attributed to less NH_4^+ oxidation

624   before freeze up in fall, resulting in more NH_4^+ remaining to drive NH_4^+ oxidation and hence

625   N_2O emissions during spring thaw. These model findings were consistent with field results from

626   Chantigny et al. (2017) in Quebec, and Kariyapperuma et al. (2012) in Ontario, where greater

627   spring N_2O emissions were measured when fall slurry was applied in late November than in

628   early November. These greater spring thaw N_2O emissions were attributed by Kariyapperuma et

629   al. (2012) to greater mineral N concentrations during spring thaw caused by less nitrification

630   before freeze up during the previous fall, as modelled here. The greater N_2O emissions modelled

631   with later slurry application were also driven by more rapid DOC oxidation from more labile

632   manure C remaining during spring thaw that reduced $[O_{2s}]$ below that simulated after earlier fall

633   applications (Fig. 3d). NI may therefore be particularly effective in reducing N_2O emissions

634   during spring thaw following late fall slurry applications.

635

636   The decreases in N_2O emissions modelled with NI from greater soil mixing (F 0.5 and F 0.8

637   *vs*. F in Table 6) were affected by how the redistribution of NI activity with soil mixing was

638   modelled. Simulating this redistribution during tillage requires further consideration and

639   corroboration from observations. These decreases in N_2O emissions with NI were associated

640   with greater N_2O emissions modelled from greater soil mixing without NI in 2016 (F 0.5 and F

641   0.8 in Table 6). These greater emissions were attributed in the model to longer periods with high

642   θ_i and low θ_g in the upper soil profile caused by greater heat loss through reduced insulation

643   from less surface litter under a shallow snow pack [D12, D13]. This longer period further

644   reduced overwinter $[O_{2s}]$ from that modelled in F (Fig. 3c), causing greater accumulation of

645   N_2O_s and hence greater emissions during thaw. These model findings were consistent with field

646   observations by Congreves et al. (2017) and Wagner-Riddle et al. (2010) that overwinter N_2O

647   emissions increased with greater freezing under conventional vs. no tillage, particularly with

648   surface residue removal. Model findings were also consistent with observations by Teepe et al.

649   (2004) that N_2O emissions during soil thawing rose sharply with increased duration of soil

650   freezing. Consequent changes in T_s with freezing may alter NI effectiveness with tillage.

651

652   **6.2.2. Spring Slurry Application**

653   Annual N_2O emissions modelled without NI from spring applications were smaller than those

654   from fall applications in 2014/2015 with a wetter early spring and drier late spring, and slightly

655   greater in 2015/2016 with a drier early spring and wetter late spring (Table 4), except when fall

656   application was delayed (e.g. F +2 in Table 6). These modelled differences in emissions were

657   consistent with experimental findings that drier springs reduce N_2O emissions from fall

658   applications relative to those from spring (e.g. Cambareri et al., 2017). These model results

659   indicate that effects of spring vs. fall slurry applications on annual N_2O emissions may not be

660   consistent, but rather will depend on the timing of fall application relative to freeze up, and on

661   precipitation during the following winter and spring.

662

663   Amendment of slurry with NI slowed declines in NH_4^+ modelled after spring applications

664   comparably to those measured (Fig. 2b). These slower declines were caused by slower NH_4^+

665   oxidation that reduced nitrifier growth (Sec. 2.9 Eq. 3) and active O_2 uptake (Sec. 2.5 step 3).

666   Consequently smaller nitrifier biomass and greater $[O_{2s}]$ were modelled with *vs*. without NI (Fig.

667   3e,g), particularly with rainfall after spring application in 2016 (Fig. 7a). The smaller nitrifier

668   biomass modelled with NI was consistent with the findings of Dong et al. (2013) that DMPP

669   reduced populations of ammonia oxidizing bacteria in soil incubations. Greater $[O_{2s}]$ modelled

670   with NI was consistent with greater $[O_{2g}]$ measured in an incubation of wetted soil amended with

671   cattle slurry with *vs*. without DMPP by Nguyen et al. (2017). Slower nitrifier growth and greater

672    $[O_{2s}]$ both contributed to reductions in N_2O emissions modelled with NI beyond those from the

673   direct effects of I_t on nitrification in Eq. 1, indicating additional effects of NI on N_2O emissions

674   that should be considered in NI models.

675

676   The reductions in N_2O emissions modelled for 30 d after spring slurry applications with R_I

677   for DMPP and nitrapyrin in 2015 (35% and 30%) and 2016 (53% and 41%) were less than those

678   measured with automated chambers (Table 5), but within the range of 31% to 44% in meta-

679   analyses of NI research by Akiyama et al. (2010) and Ruser and Schultz (2015). The greater

680   reductions modelled in 2016 *vs*. 2015 (Fig. 7 *vs*. Fig. 6) were consistent with findings in meta-

681   analyses by Akiyama et al. (2010) and Gilsanz et al. (2016) that NI was more effective in

682   reducing N_2O emissions from a given land use when emissions were greater. These greater

683   reductions were attributed in the model to heavy rainfall several days after application in 2016

684   (Fig. 7a) that extended the N_2O emission period (Fig. 7b). During this extension I_t remained high

685   because $[NH_4^+]$ had declined from the large values modelled immediately after application (Eq.

686   3).

687

688   The effects of NI on N_2O emissions modelled with greater soil mixing during spring

689   applications (S 0.5 and S 0.8 *vs*. S in Table 6) were affected by how the redistribution of NI

690   activity with soil mixing was modelled, as were those during fall applications. The effects of soil

691   mixing on N_2O emissions without NI modelled from slurry applications in spring were smaller

692   than those in fall in the absence of soil freezing effects on O_{2s}. These smaller effects were

693   modelled because tillage in this study involved mixing of injected manure rather than

694   incorporation of surface-applied manure. These small effects were consistent with an observation

695   by VanderZaag et al. (2011) that tillage was less important than timing and placement for N_2O

696   emissions from slurry applications.

697

698   The reductions in annual N_2O emissions modelled after spring slurry applications with R_I for

699   DMPP and nitrapyrin in 2015 (22% and 17%) and 2016 (40% and 27%) (Table 6) were smaller

700 than those modelled after 30 d (Table 5) due to gradual degradation of NI effectiveness modelled

701 with time since application (Eq. 1), indicating the importance of year-round modelling and

702 measurements to fully assess NI effects on N_2O emission factors for IPCC Tier 3 methodology.

703 However most of the datasets used in meta-analyses of these assessments did not include

704 emissions during autumn, winter and spring thaw (Ruser and Schulz, 2015) which are

705 particularly important for estimating emission factors for NI effects from fall slurry applications

706 in cold climates (Table 6). Ecosystem modelled with well tested simulation of NI effects may

707 make a valuable contribution to these assessments.

708

709 **6.3. Modelling NI Effects on NH_3 Emissions and Mineral N Losses**

710 The small NH_3 emissions modelled from slurry injection with limited soil mixing (Table 7)

711 were consistent with observations of almost no NH_3 volatilization from closed-slot injection of

712 slurry by Rodhe et al. (2006). In the model, NH_3 emissions with or without NI were sharply

713 reduced by NH_4^+ adsorption (Sec. 2.10) with diffusion of NH_3 and NH_4^+ from the injection site

714 (Sec. 2.11). Greater soil mixing brought more NH_4^+ closer to the surface, reducing NH_4^+

715 adsorption and thereby increasing NH_3 emission, particularly from fall applications with NI

716 (Table 7). Consequently only small net increases in NH_3 emissions (Table 7) were modelled

717 with NI from increased volatilization of aqueous NH_3 (Sec. 2.11 step 1) in equilibrium with

718 increased NH_4^+ concentrations (Fig. 2). However these increases were large in relative terms

719 particularly following fall applications, consistent with increases of $33 - 67\%$ and $3 - 65\%$

720 relative to emissions without NI derived from meta-analyses of field experiments by Qiao et al.

721 (2015) and Lam et al. (2017) respectively. Increases in NH_3 emissions with NI will thus depend

722 on soil adsorptive properties and depth of slurry incorporation.

723

724 The small losses of NO_3^-, and consequently the small reductions in these losses with NI,

725 modelled in the subhumid climate at the Edmonton South Farm (Table 7) conform to the

726 assumption by De Klein et al. (2006) that NO_3^- leaching is an insignificant source of indirect

727 N_2O emission from dryland cropping systems in subhumid climates. Consequently reductions in

728 leaching have minimal impact on the overall effect of NI on N_2O emission in these climates

729 (Lam et al., 2017). Reductions in NO_3^- losses modelled with NI would be larger at sites with

730 better drainage and more excess precipitation, although even under these conditions such

731 reductions may be small and inconsistent (Smith et al., 2002).

732

733 The increases in NH_3 emissions modelled with NI were larger than reductions in NO_3^-

734 leaching (Table 7), indicating that net increases in N_2O emissions from indirect effects of NI will

735 partially offset decreases in N_2O emissions from direct effects. This offset must be included

736 when estimating changes in N_2O emission factors attributed to NI in IPCC Tier 3 methodology.

737

6.4. Modelling NI Effects on N_2O Emissions: Parameter Evaluation

739 The simulation of N_2O emissions from nitrification and denitrification in *ecosys* is based on a

740 comprehensive representation of biological and physical processes governing production and

741 transport of N_2O. Parameters used in these processes are well constrained from basic research so

742 that the model may provide a robust means to predict emissions under diverse climates, soils and

743 land use practices. These processes in *ecosys* were not changed when adding the algorithm for

744 inhibiting NH_4^+ oxidation by nitrifiers proposed in Eqs. 1 and 2 (Sec. 2.9). This algorithm used

745 three parameters, $I_{t=0}$ and R_I in Eq. [1] and K_{iNH4} in Eq. [2] with values of 1.0, 2.0 x 10^{-4} h^{-1}, and

746 7000 g N m^{-3} to simulate the time course of NI activity following slurry application. The first

747 two parameters correspond to ones in earlier models of NI for inhibition effectiveness (0.5 – 0.9)

748 and duration (30 – 60 days) (Cui et al., 2014; Del Grosso et al., 2009). These models have given

749 reductions in N_2O emissions with NI in agricultural crops of *ca*. 25% (Cui et al., 2014), 10%

750 (Del Grosso et al., 2009) or less (Abalos et al., 2016), that are frequently smaller than reductions

751 of 26% – 43% and 24% – 46% derived from meta-analyses of NI effects in agricultural crops by

752 Akiyama et al. (2010) and Gilsanz et al. (2016) respectively.

753

754 Each of the parameters used to model NI in *ecosys* requires further evaluation. A larger R_I,

755 such as that used for nitrapyrin *vs*. DMPP (Sec. 2.9), caused a more rapid decline of NI activity

756 in soil, and hence greater N_2O emissions with time after slurry application that were consistent

757 with measurements (Tables 5 and 6; Lin et al., 2018). This larger value might represent more

758 rapid degradation of nitrapyrin through volatilization (Ruser and Schulz, 2015), although meta-

759 analyses of N_2O reductions with NI indicate that those with nitrapyrin are similar to those with

760 DMPP. The value of R_I used for NI in the model will thus likely be product specific. The effect

Biogeosciences
Discussions
EGU
Open Access

26

761   of T_s on R_I might reasonably be represented by f_{Ts} as is the effect of T_s on all other biological

762   reactions in the model. This function allowed modelled NI activity to persist overwinter (Fig. 2)

763   and hence reduce N_2O emissions modelled during spring thaw (Fig. 6 and Fig. 7). However the

764   effects of temperature on reductions in N_2O emission with NI over time are sometimes unclear in

765   controlled studies (Kelliher et al., 2008).

766

767   The value of $I_{t=0}$ set the value of I_t at the time of slurry application, after which I_t

768   underwent first order decline over time according to Eq. 1 (Sec. 2.9). However I_t had to remain

769   large enough to reduce N_2O emissions from nitrification for several weeks after application

770   (Figs. 6 and 7) even with higher soil NH_4^+ concentrations (Fig. 2). Lowering $I_{t=0}$ from 1.0 to 0.8,

771   similar to that in earlier NI models in which I_t decline was not simulated, increased N_2O

772   emissions modelled over 30 days after spring slurry applications by 7% in 2015 and 25% in 2016

773   (Table 9).

774   The value of K_{iNH4} in Eq. 2 reduced I_t with the very large NH_4^+ concentrations modelled

775   immediately after injecting slurry with large NH_4^+ content (Table 3) into small bands (Sec. 3.1).

776   The use of K_{iNH4} was suggested by the findings of Janke et al. (2019) that NI may not have the

777   expected impacts on N transformations and availability when applied in a concentrated band

778   with large NH_4^+ concentrations (up to 12 kg N Mg^{-1}), similar to those modelled immediately

779   after slurry application in this study. The modelled NH_4^+ concentrations declined rapidly after

780   application through diffusion (Sec. 2.11), adsorption (Sec. 2.10) and nitrification (Sec. 2.5), and

781   thus so did K_{iNH4} effects on inhibition. The value of K_{iNH4} in Eq. 2 therefore governed NI effects

782   modelled during the brief periods of rapid N_2O emissions following application (*ca*. 3 days in

783   Figs. 6 and 7), but had sharply diminishing impacts on NI effects modelled thereafter. An

784   alternative hypothesis for reduced inhibition by NI immediately after application might be more

785   rapid diffusion of NH_4^+ than NI from the band, leading to spatial separation (Ruser and Schulz,

786   2015), although parameterization of this hypothesis is uncertain. Halving or doubling K_{iNH4} from

787   the value set in Sec. 2.9 raised or lowered N_2O emissions modelled over 30 days after spring

788   slurry applications by 7 – 8% in 2015 and 2016 (Table 9), indicating some latitude in evaluating

789   this parameter.

Biogeosciences
Discussions

Open Access

EGU

27

790   Reductions in N$_2$O emissions modelled with all proposed values of $I_{t=0}$ and K_{iNH4} varied from

791   27% to 41% in 2015, and from 38% to 57% in 2016 (Table 9), close to the range of 42.6% ±

792   5.5% derived from meta-analyses of NI effects with cattle slurry by Gilsanz et al. (2016). Further

793   evaluation of these parameters should be undertaken in future studies in which measurements are

794   taken at higher frequencies (e.g. Figs. 6 and 7) required to assess N$_2$O emissions and NI effects

795   on them.

796

7. CONCLUSIONS

798   (a) A simple, time-dependent algorithm for adding NI effects on N$_2$O emissions into the

799   existing model *ecosys* has been presented.

800   (b) The direct effect of NI on N$_2$O emissions in the model was confined to the inhibition

801   of NH$_4^+$ oxidation

802   (c) Additional effects of NI on N$_2$O emissions were caused by slower nitrifier growth and

803   O$_2$ uptake

804   (d) Slower nitrification modelled with this algorithm caused increases in soil NH$_4^+$

805   concentrations and reductions in soil NO$_3^-$ concentrations and N$_2$O fluxes that were

806   consistent with those measured following fall and spring applications of slurry over

807   two years.

808   (e) NI in the model remained effective in reducing N$_2$O emissions modelled during

809   spring thaw, particularly when these emissions were increased by delaying fall slurry

810   applications or increasing fall tillage intensity

811   (f) NI in the model increased NH$_3$ emissions more than it reduced NO$_3^-$ leaching, causing

812   indirect effects on N$_2$O emissions that partially offset direct effects.

813   (g) NI had no significant effect on modelled or measured barley silage yields.

814   (h) Some further work is needed to corroborate parameters in the NI algorithm under a

815   wider range of site conditions.

816   (i) The addition of NI to *ecosys* may allow emission factors for different NI products to

817   be derived from annual N$_2$O emissions modelled under diverse site, soil, land use and

818   weather as required in IPCC Tier 3 methodology.

819

28

ACKNOWLEDGEMENTS

826

LIST OF REFERENCES

827

828 Abalos , D., Smith, W.N., Grant, B.B., Drury, C.F., MacKell, S. and Wagner-Riddle, C.:

829   Scenario analysis of fertilizer management practices for N_2O mitigation from corn

830   systems in Canada. Science of the Total Environ. 573, 356–365, 2016.

831 Akiyama, H., Yan, X. and Yagi, K.: Evaluation of effectiveness of enhanced efficiency fertilizers

832   as mitigation options for N2O and NO emissions from agricultural soils: Meta-analysis.

833   Glob. Change Biol. 16,1837–1846. doi:10.1111/j.1365-2486.2009.02031.x, 2010.

834 Cambareri, G., Drury, C., Lauzon, J., Salas, W. and Wagner-Riddle, C.: Year-round nitrous

835   oxide emissions as affected by timing and method of dairy slurry application to corn. Soil

836   Sci. Soc. Am. J. 81, 166–178, 2017.

837 Chantigny, M.H., Rochette, P., Angers, D.A., Goyer,C., Brin, L.D. and Bertrand. N.:

838   Nongrowing season N_2O and CO_2 emissions − Temporal dynamics and influence of soil

839   texture and fall-applied slurry. Can. J. Soil Sci. 97(3), 452-464, 2017.

840 Congreves, K.A., Brown, S.E., Németh, D.D., Dunfield K.E. and Wagner-Riddle, C.:

841   Differences in field-scale N_2O flux linked to crop residue removal under two tillage

842   systems in cold climates. GCB Bioenergy 9, 666–680, doi: 10.1111/gcbb.12354, 2017.

843 Cui, F., Zheng, X., Liu, C., Wang, K., Zhou, Z. and Deng, J.: Assessing biogeochemical effects

844   and best management practice for a wheat−maize cropping system using the DNDC

845   model. Biogeosci. 11, 91−107, 2014.

846 De Klein C, Novoa, R.S.A., Ogle, S. et al.: N_2O emissions from managed soils, and CO_2

847   emissions from lime and urea application. Chapter 11. In: 2006 IPCC Guidelines for

29

848   National Greenhouse Gas Inventories (eds Eggleston HS, Buendia L, Miwa K, Ngara T,
849   Tanabe K). IGES, Hayama, Japan, 2006.
850 Del Grosso, S.J., Ojima, D.S., Parton, W.J., Stehfest, E., Heistemann , M., DeAngelo, B. and
851   Rose, S.: Global scale DAYCENT model analysis of greenhouse gas emissions and
852   mitigation strategies for cropped soils. Global and Planetary Change 67, 44–50, 2009.
853 Dong, X.X., Zhang, L.L., Wu, Z.J., Zhang, H.W. and Gong, P.: The response of nitrifier, N-fixer
854   and denitrifier gene copy numbers to the nitrification inhibitor 3,4-dimethylpyrazole
855   phosphate . Plant, Soil Environ. 59(9), 398-403, 2013
856 Dungan, R.S., Leytem, A.B., Tarkalson, D.D., Ippolito, J.A. and Bjorneberg, D.L.: Dairy forage
857   rotation as influenced by fertilizer and slurry applications. Soil Sci. Soc. Amer. J. 81,
858   537–545, 2017.
859 Focht, D.D. and Verstraete, W.: Biochemical ecology of nitrification and denitrification. Adv.
860   Micro. Ecol. 1, 135-214, 1977.
861 Gao, W. and Bian, X.: Evaluation of the agronomic impacts on yield-scaled N_2O emission from
862   wheat and maize fields in China. Sustainability 9, 1201; doi:10.3390, 2017.
863 Gilsanz, C., Báez, D., Misselbrook,T.H., Dhanoa, M.S. and Cárdenas, L.M.: Development of
864   emission factors and efficiency of two nitrification inhibitors, DCD and DMPP. Agric,
865   Ecosyst. Environ. 216, 1-8, 2016.
866 Giltrap, D.L., Saggar, S., Singh, J., Harvey, M., McMillan, A, and Laubach, J.: Field-scale
867   verification of nitrous oxide emission reduction with DCD in dairy-grazed pasture using
868   measurements and modelling. Soil Res. 49, 696–702 http://dx.doi.org/10.1071/SR11090,
869   2011.
870 Grant, R.F.: A technique for estimating denitrification rates at different soil temperatures, water
871   contents and nitrate concentrations. Soil Sci. 152, 41-52, 1991
872 Grant, R.F.: Simulation of ecological controls on nitrification. Soil Biol. Biochem. 26, 305-315,
873   1994.
874 Grant, R.F.: Mathematical modelling of nitrous oxide evolution during nitrification. Soil Biol.
875   Biochem. 27, 1117-1125, 1995.
876 Grant, R.F. and Pattey, E.: Mathematical modelling of nitrous oxide emissions from an
877   agricultural field during spring thaw. Global Biogeochem. Cycles. 13, 679-694, 1999.

Biogeosciences

Discussions

Open Access

EGU

30

878   Grant, R.F. and Pattey, E.: Temperature sensitivity of N_2O emissions from fertilized agricultural
879   soils: mathematical modelling in *ecosys.* Global Biogeochem. Cycles 22, GB4019,
880   doi:10.1029/2008GB003273, 2008.
881   Grant, R.F., Pattey, E.M., Goddard, T.W., Kryzanowski, L.M. and Puurveen, H. Modelling the
882   effects of fertilizer application rate on nitrous oxide emissions from agricultural fields.
883   Soil Sci Soc. Amer. J. 70,: 235-248, 2006.
884   Grant, R.F., Neftel, A. and Calanca, P.: Ecological controls on N_2O emission in surface litter and
885   near-surface soil of a managed pasture: modelling and measurements. Biogeosci. 13,
886   3549–3571, 2016.
887   Guardia, G., Cangani, M.T., Sanz-Cobena, A., Junior, J.L. and Vallejo, A.: Management of pig
888   slurry to mitigate NO and yield-scaled N_2O emissions in an irrigated Mediterranean crop.
889   Agric. Ecosyst. Environ. 238, 55-66, 2017.
890   Guardia, G., Marsden, K.A., Vallejo, A., Jones, D.L. and Chadwick, D.R.: Determining the
891   influence of environmental and edaphic factors on the fate of the nitrification inhibitors
892   DCD and DMPP in soil. Sci. Total Environ. 624, 1202-1212, 2018.
893   IPCC. 2019. 2019 Refinement to the 2006 IPCC guidelines for national greenhouse gas
894   inventories. https://www.ipcc.ch/. accessed 9 July 2019.
895   Janke, C.K., Fujinuma, R., Moody, P. and Bell, M.J.: Biochemical effects of banding limit the
896   benefits of nitrification inhibition and controlled-release technology in the fertosphere of
897   high N-input systems. Soil Res. 57, 28–40 https://doi.org/10.1071/SR18211, 2019.
898   Kariyapperuma, K. A., Furon, A. and Wagner-Riddle, C.: Non-growing season nitrous oxide
899   fluxes from an agricultural soil as affected by application of liquid and composted swine
900   slurry. Can. J. Soil Sci. 92, 315,327, 2012.
901   Kelliher, F. M., Clough, T.J., Clark, H., Rys,G. and Sedcole,J.R.: The temperature dependence of
902   dicyandiamide (DCD) degradation in soils: a data synthesis. Soil Biol. Biochem. 40, 878–
903   1882, 2008.
904   Lam S.K., Suter, H., Mosier, A.R. and Chen, D.: Using nitrification inhibitors to mitigate
905   agricultural N_2O emission: a double-edged sword? Global Change Biol. 23, 485–489,
906   2017.

31

907   Lam, S.K., Suter, H., Davies, R., Bai, M., Mosier, A.R., Sun, J. and Chen, D.: Direct and indirect
908   greenhouse gas emissions from two intensive vegetable farms applied with a nitrification
909   inhibitor. Soil Biol. Biochem. 116, 48-51, 2018.

910   Lin, S., Hernandez-Ramirez, G., Kryzanowski, L., Wallace, T., Grant, R., Degenhardt, R.,
911   Berger, N., Lohstraeter , G. and Powers, L.-A.: Timing of Slurry Injection and
912   Nitrification Inhibitors Impacts on Nitrous Oxide Emissions and Nitrogen
913   Transformations in a Barley Crop. Soil Sci. Soc. Amer. J. 81,1595-1605
914   doi:10.2136/sssaj2017.03.0093, 2018.

915   Merino, P., Menéndez, S., Pinto, M., González-Murua, C. and Estavillo, J.M.: 3, 4-
916   Dimethylpyrazole phosphate reduces nitrous oxide emissions from grassland after slurry
917   application. Soil Use Manage. 21, 53–57, 2005.

918   Metivier, K.A., Pattey, E. and Grant, R.F.: Using the *ecosys* mathematical model to simulate
919   temporal variability of nitrous oxide emissions from a fertilized agricultural soil. Soil
920   Biol. Biochem. 41, 2370–2386, 2009.

921   Nguyen, Q.V., Wu, D., Kong, X., Bol, R., Petersen, S.O., Jensen, L.S., Liu, S., Brüggemann, N.,
922   Glud, R.N., Larsen, M. and Bruun, S.: Effects of cattle slurry and nitrification inhibitor
923   application on spatial soil-dynamics and N_2O production pathways. Soil Biol. Biochem.
924   11, 200-209, 2017.

925   Owens, J., Clough, T.J., Laubach, J., Hunt, J.E. and Venterea, R.T.: Nitrous oxide fluxes and soil
926   oxygen dynamics of soil treated with cow urine. Soil Sci. Soc. Amer. J. 81, 289-298,
927   doi:10.2136/sssaj2016.09.0277, 2017.

928   Qiao C., Liu, L., Hu, S., Compton, J.E., Greaver, T.L. and Li, Q.: How inhibiting nitrification
929   affects nitrogen cycle and reduces environmental impacts of anthropogenic nitrogen
930   input. Global Change Biol. 21,1249–1257, 2015.

931   Pfab, H., Palmer, I., Buegger, F., Fiedler, S., Muller, T. and Ruser, R.: Influence of a nitrification
932   inhibitor and of placed N-fertilization on N_2O fluxes from a vegetable cropped loamy
933   soil. Agric. Ecosyst. Environ. 150, 91– 101, 2012.

934   Rochette, P., Angers, D.A., Chantigny, M.H., Bertrand, N. and Côté, D.: Carbon dioxide and
935   nitrous oxide emissions following fall and spring applications of pig slurry to an
936   agricultural soil. Soil Sci. Soc. Amer. J. 68,1410–1420, 2004.

Biogeosciences
Discussions

Open Access

EGU

32

937   Rodhe, L., Pell, M. and Yamulki, S.: Nitrous oxide, methane and ammonia emissions following
938   slurry spreading on grassland. Soil Use Manage. 22, 229–237. doi:10.1111/j.1475-
939   2743.2006.00043.x, 2006.

940   Ruser, R. and Schulz, R.: The effect of nitrification inhibitors on the nitrous oxide (N_2O) release
941   from agricultural soils—a review. J. Plant Nutr. Soil Sci. 178, 171–188, 2015.

942   Smith, K. A., Beckwith, C. P., Chalmers, A. G., Jackson, D. R.: Nitrate leaching following
943   autumn and winter application of animal manures to grassland. Soil Use Manage. 18,
944   428–434, 2002.

945   Subbarao G.V., Ito, O., Sahrawat, K.L. et al.: Scope and strategies for regulation of nitrification
946   in agricultural systems: challenges and opportunities. Crit. Rev. Plant Sci. 25, 303–335,
947   2006.

948   Teepe, R., Vor, A., Beese, F. and Ludwig, B.: Emissions of N_2O from soils during cycles of
949   freezing and thawing and the effects of soil water, texture and duration of freezing. Euro.
950   J. Soil Sci. 55, 357–365, 2004.

951   VanderZaag, A.C., Jayasundara, S. and Wagner-Riddle, C.: Strategies to mitigate nitrous oxide
952   emissions from land applied manure. Animal Feed Sci. Tech. 166–167, 464-479, 2011.

953   Wagner-Riddle, C., Rapai, J., Warland, J. and Furon, A.: Nitrous oxide fluxes related to soil
954   freeze and thaw periods identified using heat pulse probes. Can. J. Soil Sci. 90, 409-418,
955   2010.

956   Wagner-Riddle, C. and Thurtell, G.W.: Nitrous oxide emissions from agricultural fields during
957   winter and spring thaw as affected by management practices. Nutr. Cycl. Agroecosyst.
958   52, 151–163, 1998.

959   Zhu, K., Bruun, S. and Jensen, L.S.: Nitrogen transformations in and N_2O emissions from soil
960   amended with slurry solids and nitrification inhibitor. Euro. J. Soil Sci. 67, 792–803.
961   2016.

Biogeosciences
Discussions

Open Access

EGU

Table 1: List of supplements in the Supporting Material

Supplement	Title	Equations
S1	Microbial C, N and P Transformations	[A1] – [A39]
S2	Soil-Plant Water Relations	[B1] – [B14]
S3	Gross Primary Productivity, Autotrophic Respiration, Growth and Litterfall	[C1] – [C53]
S4	Soil Water, Heat, Gas and Solute Fluxes	[D1] – [D21]
S5	Solute Transformations	[E1] – [E57]
S6	Symbiotic N_2 Fixation	[F1] – [F26]
S7	CH_4 Production and Consumption	[G1] – [G27]
S8	Inorganic N Transformations	[H1] – [H21]

962

Biogeosciences
Discussions

EGU

Open Access

963 **Table 2:** Key soil properties of the Black Chernozem soil at the South Edmonton Farm used in

964 *ecosys.*

Depth	BD	FC	WP	Ksat	Sand	Silt	Clay	pH	SOC	SON
m to bottom	Mg m^{-3}	m^3 m^{-3}		mm h^{-1}	g kg^{-1} mineral soil				g kg^{-1} soil	
0.01	1.15	0.34	0.15	18.0	280	450	270	6.3	57.1	5.74
0.025	1.15	0.34	0.15	18.0	280	450	270	6.3	57.1	5.74
0.05	1.15	0.34	0.15	18.0	280	450	270	6.3	57.1	5.74
0.10	1.15	0.34	0.15	18.0	280	450	270	6.3	57.1	5.74
0.15	1.35	0.34	0.15	18.0	280	450	270	6.3	40.7	3.80
0.30	1.40	0.34	0.15	7.5	250	470	280	6.3	40.7	3.80
0.60	1.50	0.35	0.17	2.5	270	420	310	7.1	3.2	0.3
0.90	1.50	0.35	0.17	2.5	270	420	310	7.1	3.2	0.3
1.20	1.50	0.35	0.17	2.5	270	420	310	7.1	3.2	0.3
1.50	1.50	0.35	0.17	2.5	270	420	310	7.1	3.2	0.3

965

35

966

967   **Table 3**. Plant and soil management schedule at the Edmonton South Campus Farm

968

Year	Date	Management	Amount			
			------------------ g N m^{-2} ------------------			g C m^{-2}
			Urea	NH$_4^+$	Organic N	Organic C
2014	15 May	fertilizer	7.2			
	15 May	planting				
	21 Aug.	harvest				
	30 Sep.	fall slurry		21.7	16.4	229.4
2015	11 May	planting				
	12 May	spring slurry		19.4	20.5	176.9
	28 Jul.	harvest				
	07 Oct.	fall slurry		21.3	19.0	198.5
2016	14 May	planting				
	16 May	spring slurry		27.2	18.6	227.5
	15 Aug.	harvest				

969

36

970

971   **Table 4**. Average temperatures and total precipitation measured at the Edmonton South Farm
972   during autumn/winter, winter/spring and spring/summer in 2014/2015 and 2015/2016.

	2014	2015		2014/5	2015	2016		2015/6
from	16 Sep	1 Jan	1 May	Average	16 Sep	1 Jan	1 May	Average
to	31 Dec	30 Apr	15 Sep	or Total	31 Dec	30 Apr	15 Sep	or Total
Temp. (^{o}C)	0.4	-1.8	16.0	**5.6**	0.8	0.1	15.8	**6.3**
Precip. (mm)	50	75	195	**320**	41	38	402	**481**

973

Biogeosciences
Discussions

Open Access

EGU

974 **Table 5**: Seasonal N_2O emissions measured and modelled during late spring in 2015 and 2016
975 without slurry (C) or with slurry applied in spring (S) without NI, with nitrapyrin or with DMPP
976 on dates in the field study (Table 3). Negative values denote emissions, positive values uptake.

977

	Year	2015		2016	
	Period	12 May – 11 June		17 May – 16 June	
		Measured	Modelled	Measured	Modelled
Treat.	Amend.	------------------------ mg N m^{-2} ----------------------			
C		+3	-1	+14	-5
S	none	-88	-89	-160	-153
S	DMPP	-48	-58	-45	-72
S	nitrapyrin	-56	-62	-57	-91

978

979

980 **Table 6**: Seasonal and annual N_2O emissions modelled during autumn/winter, winter/spring and
981 spring/summer in 2014/2015 and 2015/2016 without slurry (C) or with slurry applied in fall (F)
982 or spring (S) without NI or with R_I for DMPP on dates in the field study (Table 3), and in fall on
983 dates 2 weeks before (F-2) or after (F+2) those in the field study, and with soil mixing during
984 slurry application (M) increased to 0.4 and 0.6 from 0.2 in the field study. Negative values
985 denote emissions.

986

	Year	2014	2015		2014/5	2015	2016		2015/6
	from	16 Sep	1 Jan	1 May	Total	16 Sep	1 Jan	1 May	Total
	to	31 Dec	30 Apr	15 Sep		31 Dec	30 Apr	15 Sep	
Treat.	Amend.	--------------------------------- mg N m^{-2} --							
C		-2	-10	-14	**-26**	-2	-11	-13	**-26**
F	none	-93	-74	-17	**-184**	-93	-74	-27	**-194**
F	DMPP	-39	-68	-29	**-136**	-41	-50	-30	**-121**
F	nitrapyrin	-50	-101	-20	**-171**	-48	-61	-29	**-136**
S	none	-2	-10	-119	**-131**	-3	-25	-182	**-210**
S	DMPP	-2	-10	-90	**-102**	-3	-18	-106	**-127**
S	nitrapyrin	-2	-10	97	**-109**	-3	-24	-126	**-153**
F -2	none	-102	-64	-17	**-183**	-137	-47	-26	**-210**
F -2	DMPP	-56	-63	-19	**-138**	-55	-34	-23	**-112**
F +2	none	-92	-111	-17	**-220**	-84	-189	-52	**-325**
F +2	DMPP	-28	-78	-39	**-145**	-29	-99	-43	**-171**
F 0.5	none	-97	-71	-16	**-184**	-93	-168	-22	**-283**
F 0.5	DMPP	-58	-77	-17	**-152**	-59	-111	-20	**-190**
F 0.8	none	-102	-81	-21	**-204**	-98	-184	-19	**-301**
F 0.8	DMPP	-65	-76	-18	**-159**	-69	-138	-18	**-225**
S 0.5	none	-2	-10	-129	**-141**	-3	-27	-168	**-198**
S 0.5	DMPP	-2	-10	-98	**-110**	-3	-21	-124	**-147**
S 0.8	none	-2	-10	-138	**-150**	-3	-25	-168	**-196**
S 0.8	DMPP	-2	-10	-102	**-114**	-3	-19	-123	**-145**

987

988

39

Table 7: Annual NO_3^- discharge and NH_3 emissions modelled from 16 Sep. to 15 Sep. in 2014/2015 and 2015/2016 without slurry (C) or with slurry applied in fall (F) or spring (S) without NI and with DMPP on dates in the field study (Table 3), and in fall on dates 2 weeks before (F-2) or after (F+2) those in the field study, and with soil mixing during slurry application (M) increased to 0.5 and 0.8 from 0.2 in the field study. For NH_3 positive values indicate deposition, negative values emission.

Treat.	Year Amend.	2014/5		2015/6	
		NH_3	NO_3^-	NH_3	NO_3^-
		--------------- mg N m^{-2} ---------------			
C		+14	277	+34	421
F	none	+7	330	+29	691
F	DMPP	-147	317	+13	662
S	none	+8	279	+21	617
S	DMPP	+4	279	+14	598
F -2	none	+4	336	+26	678
F -2	DMPP	-9	326	+12	658
F +2	none	+3	336	+28	697
F +2	DMPP	-194	321	+10	662
F 0.5	none	-9	321	+17	558
F 0.5	DMPP	-79	314	-3	554
F 0.8	none	-34	500	+1	368
F 0.8	DMPP	-101	473	-29	370
S 0.5	none	-3	279	+1	490
S 0.5	DMPP	-7	279	-8	493
S 0.8	none	-15	279	-15	361
S 0.8	DMPP	-21	279	-26	365

998 **Table 8**: Barley silage yields modelled and measured without slurry (C) or with slurry applied in

999 fall (F) or spring (S) with and without NI applied on dates in the field study (Table 3)

	Year	2015		2016	
Treat.	Amend.				
		Mod.	Mes. [†]	Mod.	Mes. [†‡]
		--------------- g C m^{-2} ---------------			
C		154	198 ± 24	128	124 ± 9
F	none	284	355 ± 4	344	242 ± 45
F	DMPP	283	360 ± 25	343	255 ± 15
S	none	293	267 ± 12	334	195 ± 33
S	DMPP	297	317 ± 17	344	189 ± 32

1000 [†] calculated as 45% DM

1001 [‡] measured yields reduced by lodging

1002

1003

Biogeosciences
Discussions
Open Access
EGU

1004 **Table 9**: Sensitivity of seasonal N$_2$O emissions modelled during late spring in 2015 and 2016 to
1005 changes in initial inhibition ($I_{t=0}$ in Eq. 1) and inhibition constant (K_{iNH4} in Eq. 2) following
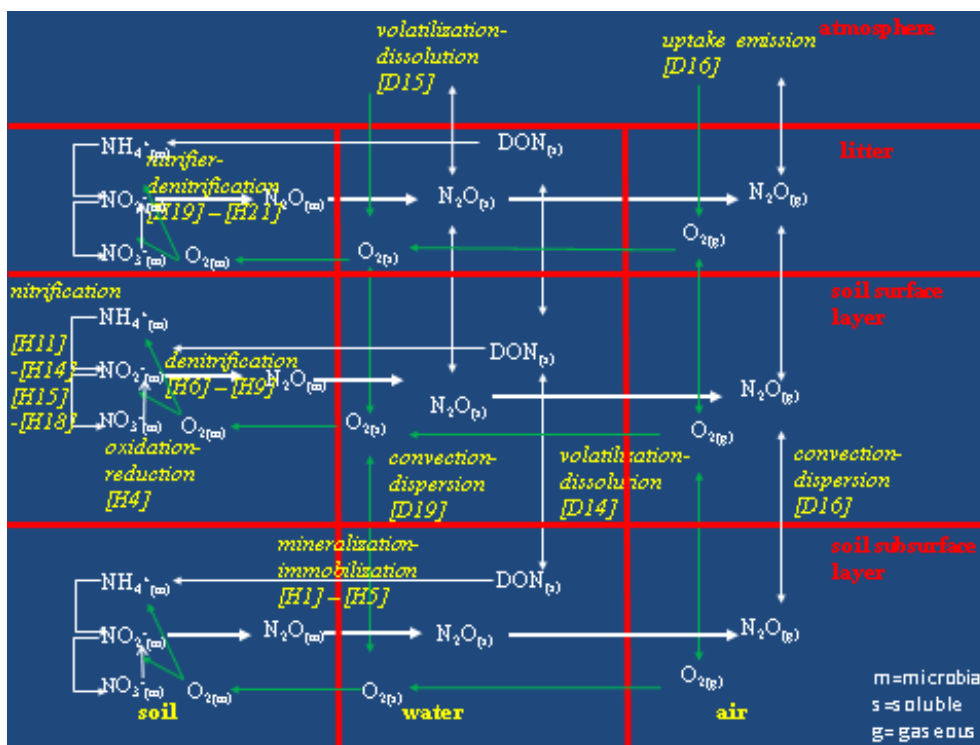1006 spring slurry application on dates in the field study (Table 3). Negative values denote emissions.

1007

Year		2015	2016
Period		12 May – 11 June	17 May – 16 June
		----------- mg N m^{-2} --------	
No NI		-89[‡]	-153[‡]
$I_{t=0}$	K_{iNH4}		
1.0	7000	-58[‡]	-72[‡]
0.9	7000	-60	-80
0.8	7000	-62	-90
1.0	3500	-62	-78
0.9	3500	-64	-86
0.8	3500	-65	-95
1.0	14000	-54	-66
0.9	14000	-57	-75
0.8	14000	-59	-85

1008 [‡] from Table 5

42

1009

1010

1011

1012 **Fig. 1**. Key transformations governing N_2O emissions as represented in *ecosys*. Expressions in

1013 square brackets refer to equations in the Supplement as described in Sec. 2.
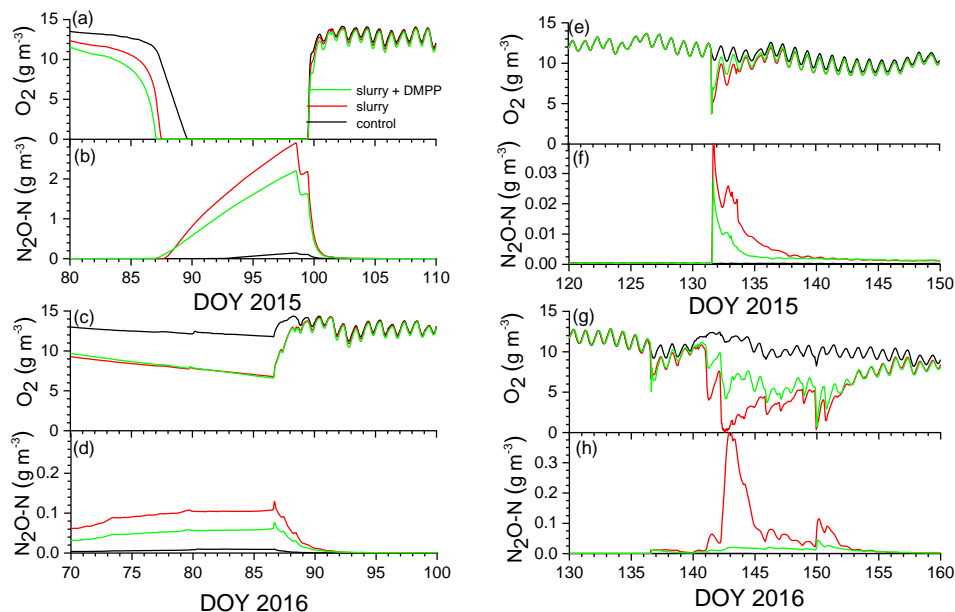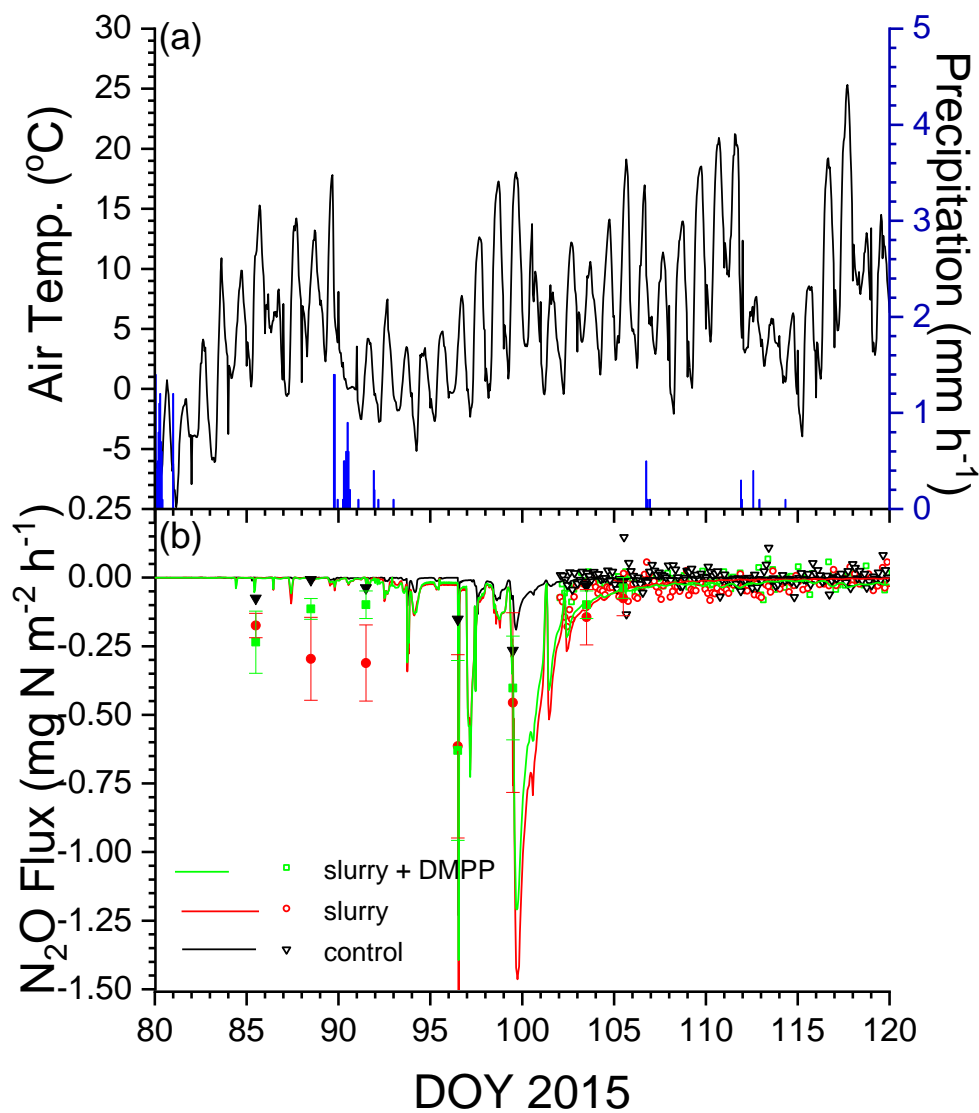
1014

43

1015

1016

Fig. 2. Soil NH_4^+ and NO_3^- concentrations measured (symbols) and modelled (lines) at $0 - 10$ cm
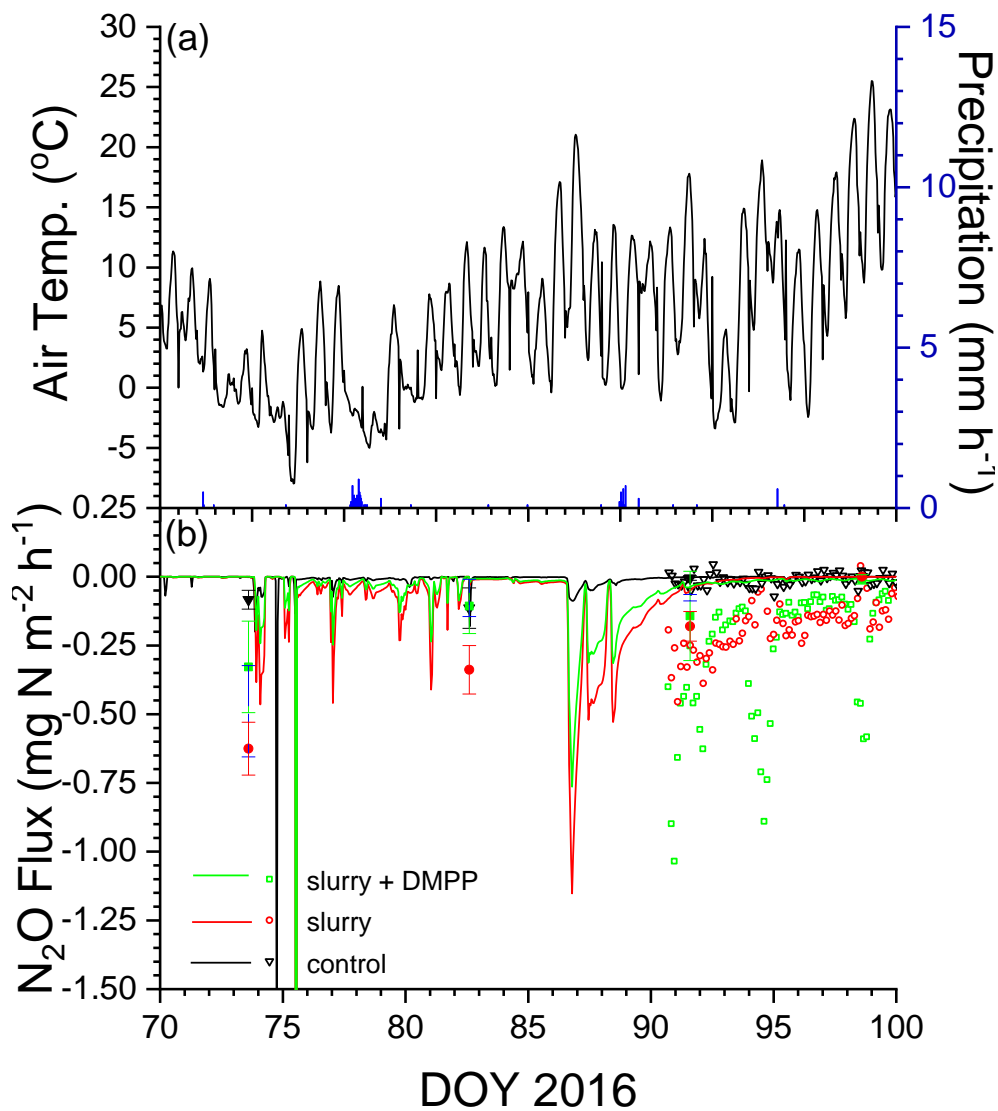depth following applications of dairy slurry without and with DMPP. Arrows indicate dates of
application.

44

1020

Fig. 3. Aqueous concentrations of O_2 and N_2O modelled at depth of slurry injection (14 cm) during emission events in early spring of (a,b) 2015 and (c,d) 2016 after fall slurry applications with or without DMPP on DOY 273 in 2014 and DOY 280 in 2015, and in later spring of (e,f) 2015 and (g,h) 2016 after spring slurry applications on DOY 132 in 2015 and DOY 137 in 2016.
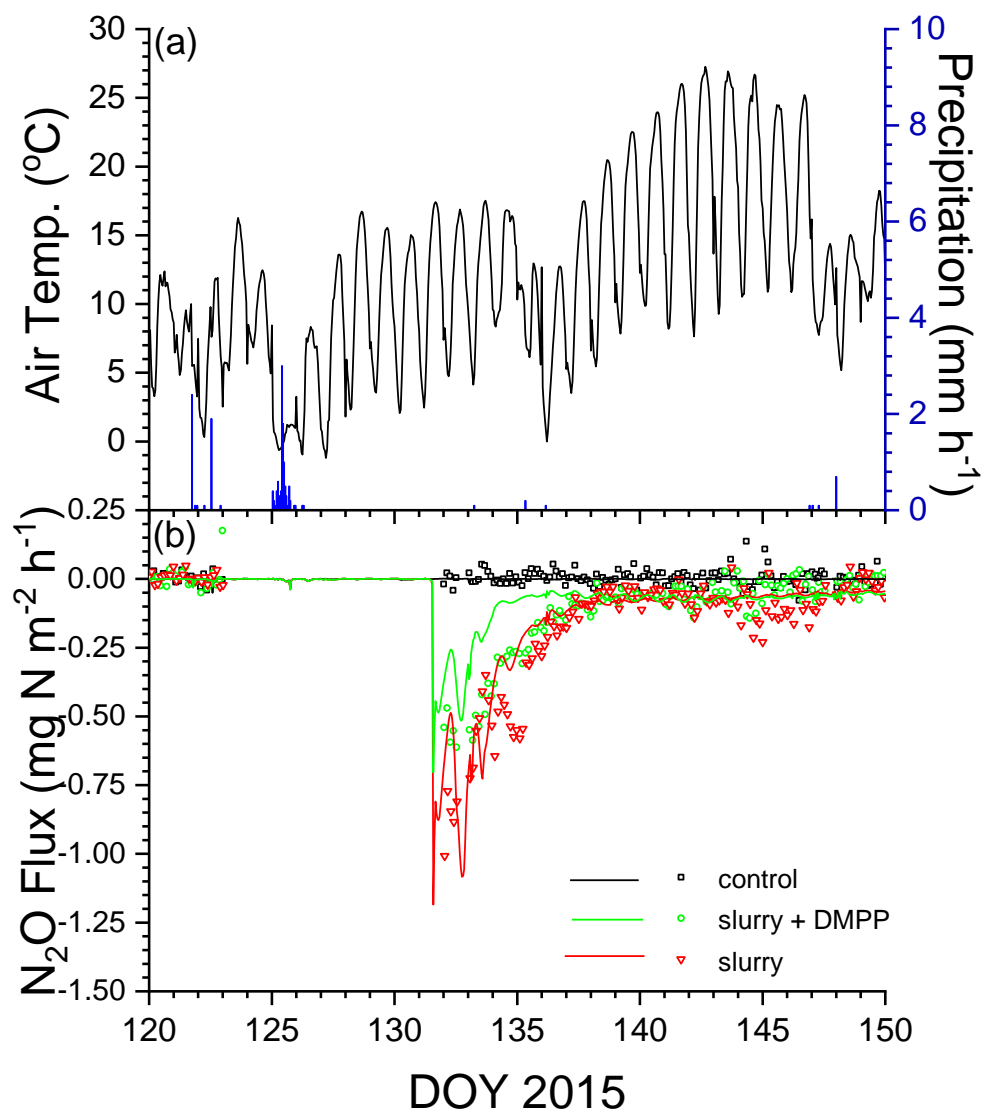
Biogeosciences

Discussions

Open Access

1025

Fig. 4. (a) Air temperature and precipitation, and (b) N$_2$O fluxes measured (symbols) and modelled (lines) during early spring 2015 with no slurry (control), and following slurry application on DOY 273 in 2014 with or without DMPP. Filled symbols represent manual chamber measurements by Lin et al. (2018). Negative values denote emissions.
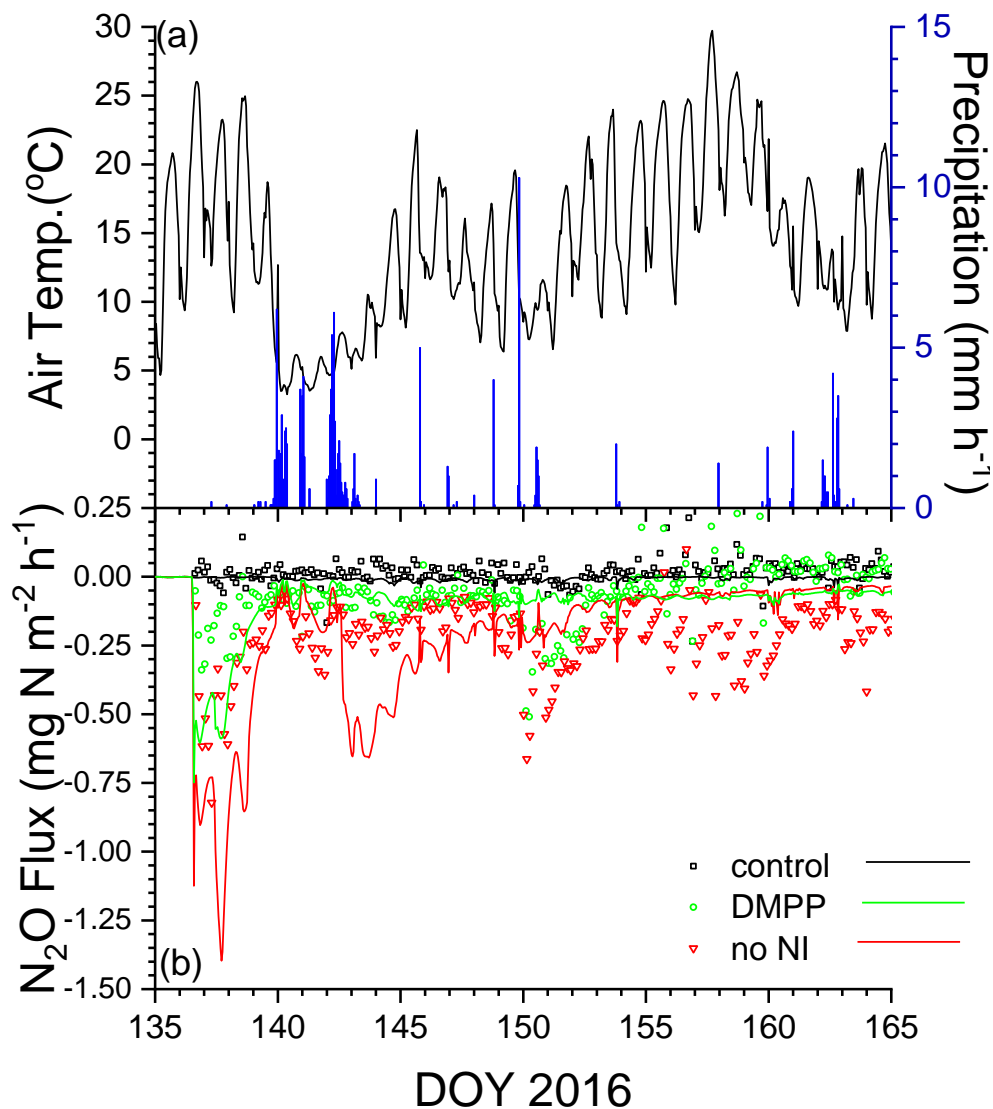
46

1030

Fig. 5. (a) Air temperature and precipitation, and (b) N$_2$O fluxes measured (symbols) and modelled (lines) during early spring 2016 with no slurry (control), and following slurry application on DOY 280 in 2015 with or without DMPP. Filled symbols represent manual chamber measurements. Negative values denote emissions.

1035

1036

1037 **Fig. 6**. (a) Air temperature and precipitation, and (b) N₂O fluxes measured (symbols) and
1038 modelled (lines) during spring 2015 with no slurry (control), and following slurry application on
1039 DOY 132 in 2015 with or without DMPP. Negative values denote emissions.

Biogeosciences
Discussions

1040

Fig. 7. (a) Air temperature and precipitation, and (b) N$_2$O fluxes measured (symbols) and
modelled (lines) during spring 2016 with no slurry (control), and following slurry application on
DOY 137 in 2016 with or without DMPP. Negative values denote emissions.

1044